

# Quarkonia and Deconfined Quark-Gluon Matter in Heavy-Ion Collisions

Anton Andronic<sup>1</sup> and Roberta Arnaldi<sup>2</sup>

<sup>1</sup>Institute for Nuclear Physics, University of Münster, Germany, 48159; email: andronic@uni-muenster.de

<sup>2</sup>INFN Sezione di Torino, Turin, Italy; email: arnaldi@to.infn.it

Xxxx. Xxx. Xxx. Xxx. YYYY. AA:1–30

[https://doi.org/10.1146/\(\(article doi\)\)](https://doi.org/10.1146/((article doi)))

Copyright © YYYY by the author(s).  
All rights reserved

## Keywords

quark-gluon plasma, heavy-ion collisions, quarkonium, charm and beauty quarks

## Abstract

In this report, we present an experimental overview of quarkonium results obtained in nucleus-nucleus heavy-ion collisions, with a focus on the data collected at the LHC. We discuss the current understanding of charmonium and bottomonium behavior in the deconfined medium produced in such collisions, comparing the various observables now accessible to state-of-the-art theoretical models. We also discuss the open points and how future heavy-ion experiments aim to clarify these aspects.

## Contents

1. INTRODUCTION .....	2
2. THEORETICAL BACKGROUND .....	3
2.1. The vacuum properties of quarkonia .....	3
2.2. General considerations .....	4
2.3. Theoretical models .....	5
3. EXPERIMENTAL OVERVIEW AND COMPARISON TO THEORY .....	9
3.1. Quarkonium observables .....	9
3.2. Collision systems for quarkonium studies .....	9
3.3. Charmonium experimental results .....	10
3.4. Bottomonium experimental results .....	19
4. WRAP UP ON CURRENT UNDERSTANDING OF QUARKONIA IN QGP .....	21
5. WHAT'S NEXT? .....	23

---

**QGP:** quark-gluon plasma is a very hot and dense medium, predicted by QCD, where quarks and gluons are no more confined into hadrons

---

**Debye screening:** Debye screening in a QGP refers to the phenomenon where the surrounding medium screens the quarks and gluons color charges due to the presence of free color charges at high temperatures. The screening length, known as Debye length, is inversely proportional to the QGP temperature.

---

## 1. INTRODUCTION

The suppression of quarkonium production was proposed almost forty years ago (1) as a unique and unambiguous signature of the formation of a plasma of quarks and gluons (QGP) in collisions of heavy nuclei at high energies (2, 3). The original idea by T. Matsui and H. Satz consisted of the assumption that the color screening (the so-called “Debye screening”), induced by the presence of a hot and dense medium, prevents the binding of the  $q$  and  $\bar{q}$  quarks forming the quarkonium, leading to a significant reduction of its production. This screening becomes stronger and stronger as the temperature of the system increases, hence the suppression is predicted to be sequential, first affecting the more loosely bound quarkonium states and only when higher temperatures are reached, also the most tightly bound states (4, 5).

The theory paper of Matsui and Satz immediately triggered the experimental search for this signature. Starting from 1986, the first studies were carried on at CERN SPS, with the NA38 experiment, investigating S-U collisions, followed shortly after by the NA50 experiment, exploiting Pb-Pb interactions, and later on, at the beginning of the year 2000, by NA60 with In-In collisions. The charmonium resonances  $J/\psi$  and  $\psi(2S)$  (i.e. the  $c$  and  $\bar{c}$  quarks bound states) were the first quarkonium states measured at the top SPS energy, at the center-of-mass energy per nucleon-nucleon collision  $\sqrt{s_{NN}} = 17.3$  GeV. Charmonium was observed to be “anomalously suppressed”, i.e. suppressed well beyond the modification induced by cold nuclear matter effects (6), leading, together with other observations carried on at the SPS, to the CERN announcement, in the year 2000, of the evidence of QGP formation in Pb-Pb collisions (7). The  $\psi(2S)$  yields in AA collisions were also observed to be more reduced with respect to the  $J/\psi$  ones, suggesting the expected sequential order in the suppression (8).

The CERN SPS results were then followed, at the beginning of the new century, by corresponding measurements at higher center-of-mass energies, firstly at RHIC at BNL (Au-Au collisions at top  $\sqrt{s_{NN}} = 200$  GeV) and later on, in 2010, at the CERN LHC (Pb-Pb collisions at top  $\sqrt{s_{NN}} = 2.76$  TeV in the so-called LHC Run1, reaching 5.02 TeV in Run2 and most recently 5.36 TeV in Run3). These higher available energies allowed to extend further the study of the QGP properties. It was soon discovered, for example,

that, with the increase of the collision energy, new mechanisms play a role. The observed suppression of the quarkonium yields, compared to the production in pp collisions, turns out to be (partially) balanced by (re)generation mechanisms (9, 10) related to the large amount of  $c\bar{c}$  quark pairs present in a deconfined medium (the number of  $c\bar{c}$  pairs,  $N_{c\bar{c}}$ , produced on average in a central collision is about 0.2 at the top SPS energy,  $\sim 10$  at RHIC and reaches  $\sim 120$  at the top LHC energy (11)). Quarks and antiquarks close in phase space can in fact combine to form a quarkonium state, either during the deconfined phase and/or at the hadronization of the system, leading to an increase of the charmonium yields.

The increase in collision energy brought further benefits to quarkonium studies. In fact, one of the peculiarities of quarkonia, is that these particles can come in a large variety of states, characterized by different binding energies and, therefore differently affected by the medium created in the heavy-ion collisions. While SPS results were limited to the  $J/\psi$  and  $\psi(2S)$ , the increase in  $\sqrt{s_{NN}}$  up to the LHC energies opened up the study of the heavier bottomonia, i.e. bound states of b and  $\bar{b}$  quarks. These measurements, previously limited by the low production cross section, now nicely complement the charmonium results.

Nowadays, at RHIC and LHC all the existing experiments pursue quarkonium measurements over (slightly) different rapidity ( $y$ ) and transverse momentum ( $p_T$ ) regions. Hence, measurements over a broad kinematic coverage are now available, allowing very detailed quarkonium studies and putting severe constraints on the theory models.

The availability of experimental results over a broad kinematic range and a wide range of collision energies, coupled with the possibility of studying a full family of particles, certainly put quarkonium in an ideal position to investigate the deconfined QGP medium, confirming its pivotal role, since now already forty years, as a signature of QGP formation.

---

**(Re)generation:** mechanism leading to the production of quarkonia due to the combination of  $q$  and  $\bar{q}$  (from the same or a different initially-produced pair) close in phase space.

---

## 2. THEORETICAL BACKGROUND

### 2.1. The vacuum properties of quarkonia

We list in **Table 1** the basic vacuum properties of the quarkonium states, both  $c\bar{c}$  and  $b\bar{b}$  families, which are currently employed for the study of the QGP (for all,  $J^{PC} = 1^{--}$ ). Here,  $\Delta m$  is the difference between the mass of the  $D, \bar{D}$  or  $B, \bar{B}$  pairs, namely the lightest mesons which contain the  $c, \bar{c}$  or  $b, \bar{b}$  quarks, respectively, and the mass of the respective quarkonium state. This quantity is a proxy for the binding energy of a given quarkonium state.

**Table 1** The vacuum properties of selected quarkonium states, the branching ratios (B.R.) into dilepton pairs, and the relative yield from feed-down (F.D.) from higher-mass quarkonium states.

State	Mass (GeV)	$\Delta m$ (GeV)	B.R.	F.D.
$J/\psi$	3.097	0.633	5.97%	30%
$\psi(2S)$	3.686	0.044	0.8%	n.a.
$\Upsilon(1S)$	9.46	1.1	2.4%	24%
$\Upsilon(2S)$	10.02	0.54	1.9%	24%
$\Upsilon(3S)$	10.36	0.21	2.2%	40%

Also listed are the branching ratios (B.R.) for the dielectron or dimuon decays, the channels in which the quarkonia are usually (in heavy-ion collisions exclusively) detected and the average fraction originating from feed-down (F.D.) through decays from higher-

mass states, either S or P states, in pp collisions (12, 13). For instance, in case of  $J/\psi$  about 8% originates from F.D. from  $\psi(2S)$  and about 22% from the  $\chi_{c1,2}$  P states (12). We note that the F.D. fractions are  $p_T$ -dependent (12, 13), listed in **Table 1** are approximate average values. We note that, for AA collisions, where the relative production rates of the various quarkonium species (within a family) are measured to be different than in pp collisions, these F.D. components will be different as well. For  $J/\psi$  and  $\psi(2S)$  mesons, an additional F.D. contribution of 10-15% and 20-30%, respectively, originates on average from hadrons containing bottom quarks; this contribution has a strong dependence on transverse momentum, being more important at high  $p_T$  (14, 15).

## 2.2. General considerations

Inclusive heavy-quark pair ( $q\bar{q}$ , where  $q$  denotes either charm or bottom) production is a perturbative QCD (hard/partonic) process, occurring in the initial phase of a nucleus-nucleus collision. The timescale of the process is of the order of  $1/2m_q$ , with  $q$  the mass of the charm and bottom quarks, about 1.5 and 5  $\text{GeV}/c^2$ , respectively. Consequently, for both charm and bottom quarks this timescale is well below  $1\text{ fm}/c$ . Quarkonium, a bound  $q\bar{q}$  state, is produced over a timescale of  $1\text{ fm}/c$  or even larger since it involves the separation of the  $q\bar{q}$  pair to reach the characteristic size of a respective quarkonium state. In heavy-ion collisions, the quarkonium formation time is comparable to (at the collider energies larger than) the time needed for the thermalization of the quark-gluon matter and the development of the collective expansion. The charm and bottom quarks are expected to thermalize slower than the bulk of the quark-gluon medium, formed by the light quarks and the gluons.

The heavy-quark potential in QGP is made quantitative through Lattice QCD (LQCD) calculations, where the complete information is encoded in the quarkonium spectral functions, see Refs. (16, 17) for reviews. The spectral functions contain information on the quarkonium binding energies and the inelastic reaction rates as a function of the temperature of the medium. The melting temperatures for various quarkonium states can also be derived, albeit in a model/procedure-dependent way. Recent LQCD calculations show that the real part of the potential, which embodies the classical screening picture, exhibits essentially no temperature dependence, while the imaginary part, which implies dissociative (collisional) processes, does depend on temperature (18). Given these considerations, the simple and attractive picture of the “quarkonium thermometer” for QGP (1, 16, 19), which is based on the screening of the real part of the potential, appears currently too simplistic. Instead, quarkonia are studied to infer their in-medium properties and the facets of the strong interaction in hot/dense QCD matter that lead to the dissociation and (re)generation processes (20). For instance, the long-range confining force was shown to be clearly modified in the QCD medium, based on the theoretical description of bottomonium data in a transport model employing a potential model (21).

The treatment of quarkonium production in theoretical approaches is intrinsically related to that of the hadrons containing open heavy quarks. Of the inclusive heavy-quark production yields only a small fraction will hadronize as quarkonia. For instance, at the LHC, in a central (0-10% class) collision about 120  $c\bar{c}$  pairs are produced on average in initial collisions in the full phase space. At midrapidity ( $y = 0$ ) there are about 16  $c\bar{c}$  pairs measured on average in one unit of rapidity, of which about 0.7% are measured in  $J/\psi$  mesons (22). Heavy quarks are overall essential probes of the QGP (17, 23, 24, 25). The

---

### Rapidity:

$$y = \frac{1}{2} \ln \frac{E - p_z}{E + p_z},$$

where  $E$  is the energy and  $p_z$  the longitudinal momentum of a particle. Quantifies the distribution of produced particles in the longitudinal (beam) direction.

---

diffusion process of heavy quarks in the QGP plays a crucial role in theoretical modeling of quarkonium production and interaction in the hot/dense QGP(17).

### 2.3. Theoretical models

Previous reviews on quarkonium production in heavy-ion collisions (16, 20, 26, 27) focused intensively on the theoretical aspects. As our review is more focused on the experimental status, we briefly review here only the main lines of current theoretical effort on the description of quarkonium in QGP. A recent comprehensive inter-comparison of various models is available in Ref. (28). There are two basic approaches for the theoretical description of quarkonium in QGP: i) the statistical hadronization model and ii) dynamical models, performing transport via either semiclassical kinetic-rate equations or in an open quantum systems framework.

**2.3.1. The Statistical Hadronization Model.** In the Statistical Hadronization Model for charm (SHMc) (9, 11, 29, 30) full dissociation of all quarkonium states in the QGP and exclusive generation at the QCD (crossover) phase boundary is assumed. This implies for heavy quarks a hadronization process which is concurrent with those of lighter quarks and gluons. At high collision energies hadronization coincides with the chemical freeze-out stage in the evolution of the hot QCD medium and with the QCD crossover transition (31), which LQCD predicts at a temperature  $T_{pc} = 156 - 158$  MeV (32, 33).

The complete thermalization of the heavy quarks in the expanding deconfined medium down to QCD crossover transition is an essential condition for the applicability of SHMc. In this approach, the knowledge of the inclusive  $q\bar{q}$  production cross-section along with the chemical freeze-out (hadronization) temperature  $T_{cf} \simeq 157 \pm 2$  MeV obtained from the analysis of the yields of hadrons composed of light quarks (31), is sufficient to determine the total ( $p_T$ -integrated) yield of all hadrons containing heavy quarks in ultra-relativistic nuclear collisions.

This is based on the balance equation relating the initial inclusive charm production to the hadronic states:

$$N_{c\bar{c}} = \frac{1}{2}g_c V \sum_i n_i^{\text{th}} \frac{I_1(N_c^{\text{tot}})}{I_0(N_c^{\text{tot}})} + g_c^2 V \sum_j n_j^{\text{th}} + \frac{1}{2}g_c^2 V \sum_k n_k^{\text{th}} \frac{I_2(N_c^{\text{tot}})}{I_0(N_c^{\text{tot}})}, \quad 1.$$

where  $N_{c\bar{c}} \equiv dN_{c\bar{c}}/dy$  denotes the rapidity density of charm quark pairs produced in initial hard collisions and the (grand-canonical) thermal densities for open and hidden charm hadrons are given by  $n_{i,j,k}^{\text{th}}$ . The index  $i$  runs over all open charm states with one valence charm or anti-charm quark ( $D, D_s, \Lambda_c, \Xi_c, \Omega_c$  and antiparticles), the index  $j$  over all quarkonium states ( $J/\psi, \chi_c, \psi(2S)$ ), and the index  $k$  over open charm states with two charm or anti-charm quarks ( $\Xi_{cc}, \Omega_{cc}$  and antiparticles). The ratio of the modified Bessel functions,  $I_\alpha/I_0$ , is a (canonical) correction for the exact conservation of charm (34, 35). The argument,  $N_c^{\text{tot}}$ , is the total charm content (particles and antiparticles), consequently containing, besides the thermal densities of charmed hadrons and the volume, the  $g_c$  factor. The thermal densities are computed in the grand canonical ensemble using the latest version of the SHMc (31, 36), with the chemical freeze-out temperature  $T_{cf} \simeq 157$  MeV. The fireball volume per unit rapidity at mid-rapidity is  $V = 4997 \pm 455$  fm<sup>3</sup> for the most central 10% Pb-Pb collisions at LHC energy  $\sqrt{s_{NN}} = 5.02$  TeV. In this case, based on the measured average value  $N_{c\bar{c}} \simeq 16$  for one unit of rapidity (22),  $g_c \simeq 31.5$ . While the thermal densities do not

---

#### QCD crossover

**transition:** is the transition between hadronic matter and QGP. According to LQCD, at baryochemical potential  $\mu_B \sim 0$  the transition is a crossover at  $T_{pc} = 156 - 158$  MeV

---

#### Chemical freeze-out:

is the stage, in the evolution of heavy-ion collisions, where the relative abundances of the different particle species are fixed.

---

---

**Centrality:** is estimated based on data and the Glauber model (38), a geometric nuclear overlap model, and expressed either as a range in the total geometric cross section or as the average number of participating nucleons,  $\langle N_{part} \rangle$ , for a given range.

---

vary with centrality of the collision,  $N_{c\bar{c}}$  and  $V$  in **Equation 1** are centrality-dependent and scale with the number of nucleon-nucleon collisions,  $N_{coll}$ , and number of participating nucleons,  $N_{part}$ , respectively. This leads to a quasi-linear dependence of  $g_c$  on  $N_{part}$ . Thermal charm production as well as charm quark-antiquark annihilation in Pb-Pb collisions are neglected, as they were estimated to be very small at the LHC energies and negligible for lower energies (11, 37).

With the assumption of the kinetic freeze-out taking place also at the QCD phase boundary and employing hydrodynamics, the transverse momentum distributions can be calculated as well (39). A corona contribution is added, both for the total and the  $p_T$ -differential yields, based on measurements in pp collisions. The SHM was applied to the bottom sector too (11, 40), although in this case the incomplete thermalization of bottom quarks needs to be considered, in addition to the primordial component.

**2.3.2. Transport Models.** In the semi-classical transport (10, 41, 42), the time evolution of the yield  $N$  for a given quarkonium species (charmonium and bottomonium) is governed by a rate equation:

$$\frac{dN(\tau(T))}{d\tau} = -\Gamma(T(\tau)) [N(\tau) - N^{eq}(T(\tau))], \quad 2.$$

where  $\tau$  is the time in the expanding fireball reference frame,  $T(\tau)$  is the local temperature,  $\Gamma$  is the reaction rate and  $N^{eq}$  is the equilibrium value for the yield. The loss term in this equation,  $-\Gamma(T(\tau))N(\tau)$ , describes the suppression of initially-produced quarkonia, while the other term is a gain term and corresponds to the (re)generation of quarkonia from  $q\bar{q}$  pairs in the medium. Here,  $q$  and  $\bar{q}$  can originate from the same initial  $q\bar{q}$  pair (a so-called “diagonal term”) or from two different initial pairs (“non-diagonal term”). The dependence  $T(\tau)$  is fixed through hydrodynamical model comparison to collective flow data at a given collision energy and for a given centrality class. For instance, for central Pb-Pb collisions (0-10%) at  $\sqrt{s_{NN}} = 5.02$  TeV,  $T$  decreases from about 600 MeV at the very early equilibrium stage ( $\tau \simeq 0.5$  fm/c) to  $T_{pc}$  at the QCD crossover boundary in about 15 fm/c (28). The reaction rate  $\Gamma$  needs to be modeled phenomenologically. The state-of-the-art such modeling employs in-medium ( $T$ -dependent) quark masses and binding energies (43), and is anchored to LQCD results (44). For instance, in the thermodynamic T-matrix approach (42, 43), the in-medium  $c$ -quark mass decreases by about 20% up to  $T = 400$  MeV and the binding energies of quarkonia decrease strongly as a function of  $T$ . Other LQCD-anchored approaches (45) employ no medium-modified quark masses or binding energies, see Ref. (28) for a comprehensive overview. The reaction rates increase significantly with  $T$  (see **Figure 1**) and show, in general, an increase with momentum. Note that Equation 2 is written in the “natural units” system, in which  $\hbar = c = 1$ . In this system of units  $\Gamma$  is GeV, and the conversion to S.I. units is:  $1 \text{ GeV} \simeq 1.5 \times 10^{24} \text{ s}^{-1}$ .

It was observed in the study of Ref. (28) that the model inputs for the reaction rates, as well as for the in-medium binding energy of the various quarkonium states, are quite different among the various model implementations, a situation that clearly needs to be improved upon. We show exemplary in **Figure 1** the temperature dependence for the reaction rates for the ground-state charmonium and bottomonium states. The reaction rates are larger for the excited states, where the spread between the values used in various models is also larger. All implementations include (re)generation, including the non-diagonal term.

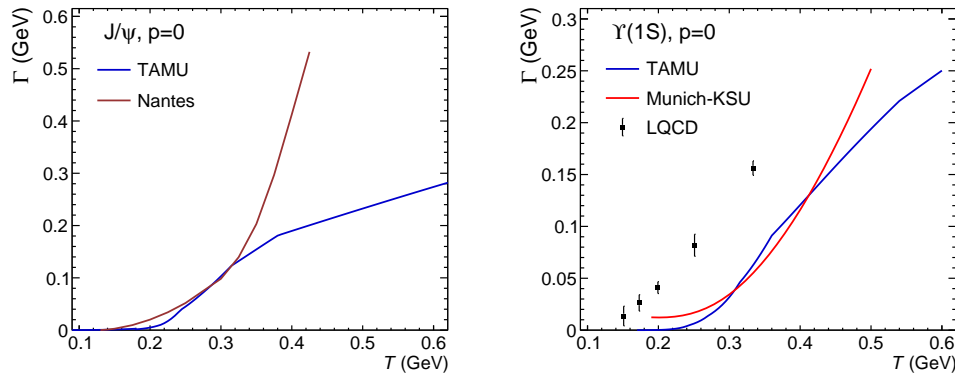


**Figure 1**

The temperature dependence of the reaction rates  $\Gamma$  for the  $J/\psi$  (left panel) and  $\Upsilon(1S)$  mesons (right panel, note the different scale of the vertical axis) at zero momentum. The values used in the semi-classical (TAMU (42)) and open-quantum systems (Nantes (46) and Munich-KSU (47)) transport approaches are shown, compared, in case of  $\Upsilon(1S)$ , with LQCD predictions (44).

Besides such transport models based on rate equations and/or semiclassical Boltzmann equations (48), transport approaches utilizing open-quantum system (OQS) frameworks have been developed in the recent years, see the review in Ref. (49). The quantum master equations can be reduced, under certain conditions, mainly in case the binding energy of the quarkonium state is (much) smaller than the temperature of the medium, to the so-called Lindblad equation. This is called the regime of the quantum Brownian motion, see discussion in Ref. (46). The hierarchy of times discussed above (and, equivalently, of energy scales) plays a role in this procedure and leads to domains of applicability of the OQS approaches (45, 46). The hierarchy is also exploited in an effective theory of the strong interaction, the (potential) non-relativistic Quantum Chromodynamics, (p)NRQCD (50), which allows the phenomenological application of OQS to quarkonium production (suppression) in the QGP (45, 49). In current quantum-transport approaches, which mostly focus on bottomonia, (re)generation is within a single  $b\bar{b}$  pair (diagonal term) and shown to be significant (47). The quantum effects appear to be significant mostly for the early stages of quarkonium evolution (28).

In **Figure 2** we illustrate the features of the SHMc and TAMU transport models concerning  $J/\psi$  production in Pb-Pb collisions at  $\sqrt{s_{NN}} = 5.02$  TeV. The SHMc describes very well the relative production of the  $J/\psi$  to  $D^0$  mesons (left panel). Given this constraint, the uncertainty in the model is largely correlated with that of the experimental data. A remarkable feature of the SHMc is that it describes the absolute yield of the  $J/\psi$  mesons, alongside that all the measured open-charm hadrons (22). The TAMU transport model predicts (right panel of **Figure 2**) that the fraction of  $J/\psi$  mesons produced through (re)generation has a centrality dependence and reaches about 80% of the total  $J/\psi$  yield in central collisions, where the initially-produced  $J/\psi$  mesons contribute only around 5%. The situation is different in mid-central collisions, where for  $\langle N_{part} \rangle \simeq 100$  the TAMU model predicts a fraction of  $J/\psi$  yield from (re)generation in QGP equal to the primordial yield, while for the SHMc all yield is newly generated in the QGP at the QCD crossover boundary. Here, the contrast between the two models is plain. For both models, a larger inclusive charm production cross section  $d\sigma_{cc}/dy$  leads to a more pronounced (re)generation

---

**Nuclear shadowing:** the reduction (saturation) of parton (gluon) densities (Parton Distribution Functions) in nuclei compared to free nucleons (52).

---



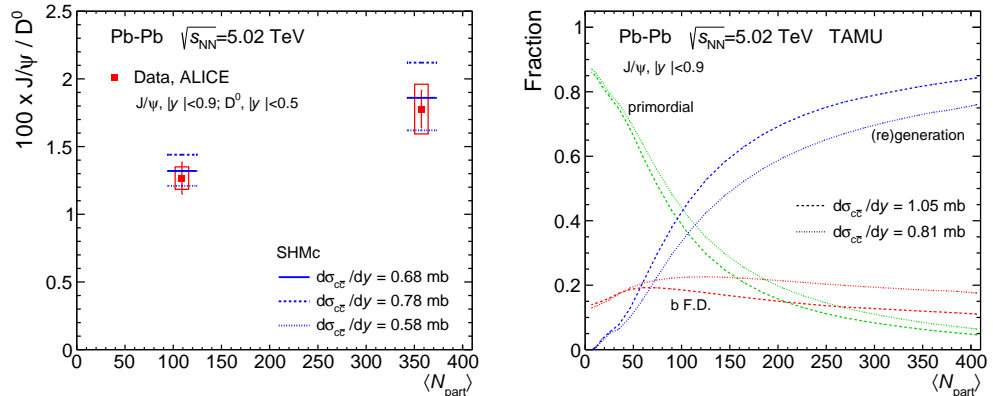


**Figure 2**

Left panel: the yield ratio  $J/\psi$  to  $D^0$  (in percent) as a function of centrality. The data from ALICE (51) are compared to the prediction of SHMc (30). Right panel: the fraction of primordial, (re)generation and F.D. from bottom hadrons for  $J/\psi$  yields as a function of centrality, calculated in the TAMU transport model (42).

of  $J/\psi$  mesons, seen for the TAMU model directly and for the SHMc meson as a larger ratio to the  $D^0$  yield. An early prediction of the transport models was that the (re)generation component is predominantly at low  $p_T$  (53) and it leads to collective flow (54).

Not only for the SHMc and TAMU models illustrated here, but in general  $d\sigma_{c\bar{c}}/dy$  is a fundamental input for the theoretical calculations for charmonium (and to some extent also bottomonium) production in QGP. The values of  $d\sigma_{c\bar{c}}/dy$  considered in the calculations shown in **Figure 2** are in fact spanning the uncertainties used in the two models for  $d\sigma_{c\bar{c}}/dy$ . Note that this is the equivalent value for pp collisions, after nuclear shadowing for Pb-Pb collisions was factored in. The SHMc and TAMU models employ two different values,  $d\sigma_{c\bar{c}}/dy = 0.68 \pm 0.10$  mb and  $d\sigma_{c\bar{c}}/dy = 0.93 \pm 0.12$  mb, respectively. The SHMc value is derived from the experimentally measured yields of  $D^0$  mesons in 0-10% Pb-Pb collisions (55) and assuming hadronization fractions as in SHMc, with an enhanced spectrum of charged baryons (30) (see also (56, 57)). The value in the TAMU model is derived from the measured value in pp collisions and assuming shadowing in the range 10-30%. This current mismatch in the input values of the two models needs to be resolved. A precise experimental evaluation of this quantity requires the measurement of all ground-state open charm mesons and baryons down to zero  $p_T$  in nuclear collisions and remains a challenge to date.

We will compare to current experimental data, with a focus on the measurements at the LHC, illustratively the SHMc, the TAMU semiclassical transport and the Munich-KSU OQS+pNRQCD models. Several other groups have made contributions and achieved a good description of (some of) the quarkonium data in the semiclassical transport (54, 58, 59, 60, 61) or quantum approaches (62, 63, 64, 65). We note that not all these models are based on the LQCD constraints mentioned above (28). A comprehensive comparison of CMS data on  $\Upsilon$  production at the LHC with theoretical models is available in Ref. (66).



### 3. EXPERIMENTAL OVERVIEW AND COMPARISON TO THEORY

As discussed, quarkonium has been one of the first observables investigated in heavy-ion collisions and the understanding of its behavior in a hot and very dense matter has gone hand in hand with the evolution of the experiments at the more and more powerful accelerators. In this report, we will outline the status of quarkonium measurements in nucleus-nucleus collisions, with emphasis on the RHIC and LHC data. A review of the SPS and early RHIC data and their theoretical interpretation is also available in Ref. (19, 29).

#### 3.1. Quarkonium observables

Several observables are used to study the quarkonium behavior in heavy-ion interactions. The most common one is the so-called nuclear modification factor,  $R_{AA}$ . In the  $R_{AA}$ , defined as  $R_{AA} = N_{J/\psi}^{AA} / (\sigma_{J/\psi}^{pp} \times \langle T_{AA} \rangle)$ , the quarkonium production yield in AA collisions ( $N_{J/\psi}^{AA}$ ) is compared to the quarkonium production cross section in proton-proton interactions ( $\sigma_{J/\psi}^{pp}$ ), scaled by the average nuclear overlap function  $\langle T_{AA} \rangle$ .  $\langle T_{AA} \rangle$  is a quantity derived from a Glauber model calculation (38) and it is proportional to the number of nucleon-nucleon collisions. Any deviation of  $R_{AA}$  from unity might indicate a modification in the production of quarkonium induced by the medium formed in the collisions.

With the availability of data from RHIC and LHC, other observables, often requiring large statistics to be studied, became of interest for quarkonium studies. As an example, observables such as the elliptic flow  $v_2$  and the polarization, provide additional information on the quarkonium behavior in heavy-ion collisions and, in particular, on the interplay between suppression and (re)generation mechanisms.

Details on the dynamics of the early stages of the collisions can, for example, be inferred from the azimuthal particle distribution. In fact, in non-central collisions, the geometrical overlap region, and hence the initial matter distribution is anisotropic. If the matter is strongly interacting, this spatial anisotropy converts, through multiple collisions, into an anisotropic particle's momentum distribution. The beam axis and the impact parameter vector of the colliding nuclei define the reaction plane and the second coefficient ( $v_2$ ) of the Fourier expansion of the particle azimuthal distribution with respect to this plane is called the elliptic flow. Charm quarks, if thermalized in the QGP, will participate to the particles flow, leading to a quarkonium  $v_2$  different from zero. Hence, the larger the fraction of  $J/\psi$  produced by (re)generation, the larger the  $v_2$  will be.

Finally, quarkonia may also exhibit polarization, defined as the alignment of the particle spin with respect to a chosen axis (67). The degree of polarization can be influenced by the presence of the quark-gluon plasma, because, for example, of the existence of a strong magnetic field in the early stage of its formation and/or because of its behavior as a rotating fluid with large vorticity. Also, in this case,  $J/\psi$  produced by (re)generation might be affected differently with respect to the primordial ones.

#### 3.2. Collision systems for quarkonium studies

In heavy-ion experiments, quarkonium is usually studied not only in nucleus-nucleus collisions (mainly Pb-Pb collisions at both SPS and LHC and Au-Au at RHIC), but also in pp and p-nucleus interactions. These topics are not extensively covered here, but are reviewed in Ref. (68).

On one side, quarkonium measurements in pp are essential to the investigation of its

---

**$R_{AA}$** : nuclear modification factor, defined as  $R_{AA} = N_{J/\psi}^{AA} / (\sigma_{J/\psi}^{pp} \times \langle T_{AA} \rangle)$

---

---

**$v_2$** : elliptic flow coefficient, is the quadrupolar term in the Fourier expansion of the azimuthal distribution of particles emission with respect to the reaction plane, determined by the beam axis and the impact parameter vector of the colliding nuclei.

---

---

**CNM effects:** initial or final state effects that modify the quarkonium yield. Their presence is related to the nuclear medium. CNM effects are always present in AA collisions, but they are usually investigated in minimum bias pA collisions, since in this lighter system hot matter effects are considered to be negligible.

---

---

**Anomalous  $J/\psi$  suppression:** this is how the NA50 experiment referred to the first observation of the suppression of the  $J/\psi$  yields in Pb-Pb collisions, beyond the modification induced by CNM effects

---

hadronic production mechanism. On the other side, since in pp collisions no QGP is expected to be formed, pp measurements represent a crucial reference for AA results, as it can be deduced from the  $R_{AA}$  definition. A very precise determination of the pp baseline, which has to be obtained at the same energy and in the same kinematic range as the AA data, is therefore mandatory for the understanding of the nucleus-nucleus results.

Already from the first quarkonium studies at CERN SPS (69, 70, 71) it was immediately realized that the quarkonium production yields are not only influenced by the hot matter formation but also by cold nuclear matter effects (CNM), associated to the presence of a nuclear medium. Effects such as the nuclear shadowing, i.e. the modification of the quark and gluon structure function for nucleons inside nuclei (see e.g. Ref. (52, 72, 73)) or the formation of a Color Glass Condensate (CGC) (74) involving low-x quarks and gluons, affect the quarkonium production in nuclear collisions. In addition to these purely initial state effects, both the incoming partons and the  $c\bar{c}$  pair propagating through the nucleus may lose energy by gluon radiation (75) at various stages of the charmonium formation process, inducing further modifications in the observed yields. Finally, the fully formed quarkonium could be dissociated via inelastic interactions with the surrounding nucleons. This final-state process, which has a dominant role among CNM effects at low collision energy (76, 77), is negligible at the LHC, where the crossing time of the two nuclei is much shorter than the formation time of the resonance (78, 79).

The CNM effects introduced above are present in nucleus-nucleus collisions, but can be investigated more directly by studying proton-nucleus collisions (or d-A collisions, in the case of RHIC experiments), where the contribution of hot-matter effects are thought to be negligible. A precise assessment of the size of CNM effects is hence mandatory, to properly establish the impact of the hot matter ones, as it will be discussed in Section 4.

### 3.3. Charmonium experimental results

$J/\psi$  was the first quarkonium state to be extensively investigated in heavy-ion collisions. The first, very precise, charmonium results at CERN SPS ( $\sqrt{s_{NN}} = 17.3$  GeV) have shown a clear “anomalous suppression” of the  $J/\psi$  yields in central Pb-Pb collisions when compared to pure CNM effects (6, 98).

Due to the unavailability of pp collisions, the  $J/\psi$  yield was studied in comparison to the Drell-Yan process, which, having an electromagnetic nature, is not affected by the QGP formation. The size of the observed suppression ( $\sim 30\%$  in the most central interactions) is quantitatively consistent with the melting of the weakly bound  $\psi(2S)$  and  $\chi_c$  states whose feed-down contributions to the  $J/\psi$  are globally of the same order. A hierarchy between the  $J/\psi$  and  $\psi(2S)$ , with the latter experiencing stronger suppression, was indeed observed by NA50 (8).

Nevertheless, on the precise nature of the medium formed in central Pb-Pb collisions at SPS energies, whether it was a deconfined one or a dense hadron gas, several discussions were triggered, due to competing theoretical models being able to describe fairly-well the charmonium data (9, 35, 41, 99, 100, 101).

With a ten times higher center-of-mass energy ( $\sqrt{s_{NN}} = 200$  GeV), the measurements of PHENIX and STAR at RHIC, confirmed the strong suppression of the  $J/\psi$  production also in Au-Au collisions, when now compared to pp (102, 103, 104, 105). The observed suppression has a similar magnitude as the one measured at SPS and it shows, for the first time, a significant rapidity dependence, being stronger at forward rapidity ( $1.2 < |y| < 2.2$ )

## QUARKONIUM IN P-P AND P-A COLLISIONS

In heavy-ion experiments, quarkonium is studied not only in AA collisions, but also in pp and pA (at SPS and LHC) or dA interactions (at RHIC). The interest in pp collisions is twofold:

- to shed light on the quarkonium hadronic production mechanisms
- as a baseline for AA results, since in minimum-bias pp collisions no medium modifications are expected

In pA collisions, quarkonium production is modified by several mechanisms (nuclear shadowing, CGC, energy loss, nuclear absorption,...) denominated cold nuclear matter effects (CNM). Quarkonium measurements in pA are hence a tool:

- to understand these effects and their complex interplay
- to quantify the size of these effects. CNM effects are present also in AA collisions, together with the hot-matter ones, so their evaluation in minimum-bias pA interactions, where no significant other effects are expected, is ideal to disentangle the QGP-related mechanisms in AA.

Quarkonium in pA has been extensively studied at LHC (80, 81, 82, 83) and RHIC (84, 85, 86). While the production of the ground states, the  $J/\psi$  and the  $\Upsilon(1S)$ , is dominated by shadowing or energy loss (87, 88, 89), the interpretation of the excited states is more complex, theoretical modeling requiring the presence of a deconfined medium in p-Pb collisions at LHC (or d-Au at RHIC) (89, 90).

On one side, the initial CNM effects, connected to the creation of the heavy-quark pair, are expected to be of a very similar size for the  $J/\psi$  and the  $\psi(2S)$ , given that the two resonances are rather close in mass. On the other side, final-state CNM effects, as the break-up of the resonance via interactions with the nucleons of the Pb nuclei, are expected to impact differently the two states, as observed at SPS energies. However, at LHC (or even RHIC) energies, these final-state effects are negligible, because of the very small time spent by the resonance in the nuclear matter. This time is evaluated as  $\tau = \langle L \rangle / \beta_z \gamma$ , with  $\langle L \rangle$  is the average length of nuclear matter crossed by the  $c\bar{c}$  pair,  $\beta_z$  is the velocity of the pair in the beam direction and  $\gamma = E_{c\bar{c}} / m_{c\bar{c}}$ , where  $m_{c\bar{c}}$  is the average mass of the evolving  $c\bar{c}$  pair (91, 92, 93). At LHC energies  $\tau$  ranges between  $7 \cdot 10^{-2} - 10^{-4}$  fm/c at low  $p_T$  (22).

Contrary to these expectations, the  $\psi(2S)$   $R_{pA}$  measurement shows a different behavior compared to the  $J/\psi$  (92, 93, 94, 95), presenting an additional suppression, in particular in the backward rapidity region. This observation is suggestive of additional final-state effects, such as interactions in a very dense medium (of hadronic or partonic origin (89, 90, 96, 97)) at play, meaning that the medium created in p(d)-A collisions might already impact the yields of the loosely bound  $\psi(2S)$ .

than at midrapidity ( $|y| < 0.35$ ). The interpretation of the RHIC results, assuming both the suppression of the tightly bound  $J/\psi$  and a contribution from (re)generation mechanisms, is not straightforward nor conclusive, due also to the complex interplay between the hot and cold matter effects.

The eagerly awaited LHC measurements, with a further increase in  $\sqrt{s_{NN}}$  by a factor initially 14, and nowadays 25, with respect to the RHIC energies and the possibility to cover a very broad rapidity range, down to very low transverse momentum, were indeed in an ideal position to clarify the observations done so far. These data were expected to shed

light on the role played by (re)generation, as the ultimate test of QGP formation.

**3.3.1.  $J/\psi$  in AA collisions.** The compilation of the  $J/\psi$  results obtained at midrapidity, at all the available nucleon-nucleon center-of-mass energies, from SPS up to LHC, is shown in **Figure 3**.

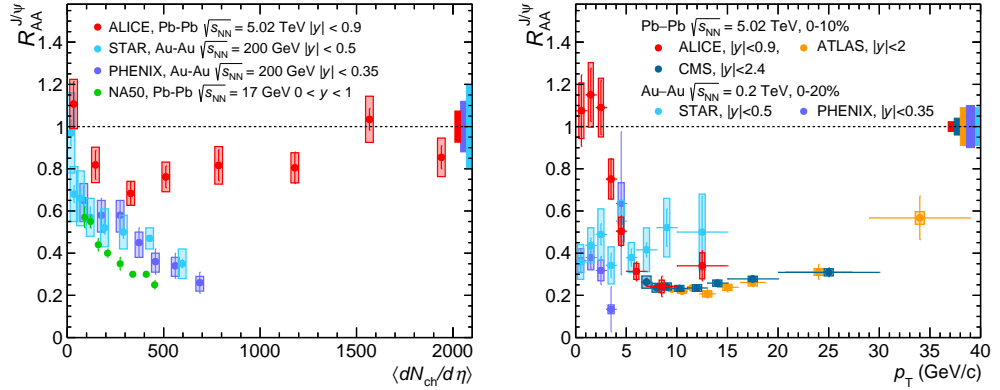


**Figure 3**

The  $J/\psi$   $R_{AA}$  for Pb–Pb collisions (51, 106, 107) at  $\sqrt{s_{NN}} = 5.02$  TeV and for Au–Au collisions at  $\sqrt{s_{NN}} = 200$  GeV (102, 105) is shown as a function of the charged particle multiplicity (left panel) and as a function of  $p_T$  (right panel). In the left panel, the SPS data from NA50 (6) (as shown in Ref. (22)) are also included. It should be noted that results from NA50, PHENIX, STAR and ALICE refer to the inclusive  $J/\psi$  production, while those from ATLAS and CMS are for prompt  $J/\psi$  only. However, since the contribution of B feed down becomes relevant only towards high  $p_T$ , the comparison between these measurements remains meaningful.

In the left panel, results are shown as a function of the mean charged particle multiplicities  $\langle dN_{ch}/d\eta \rangle$  measured at  $\eta = 0$ . In each collision system, this quantity is directly related to the centrality of the interactions and it is a useful variable to compare different collision systems since it is roughly proportional to the initial energy density. At SPS and RHIC energies, the  $J/\psi$   $R_{AA}$  decreases when moving from peripheral to central collisions, with a hint of stronger reduction in the SPS results. When moving to the higher LHC energies, two striking features appear in the  $R_{AA}$  pattern. On one side the suppression effects are almost vanishing, in particular towards central collisions, where the  $R_{AA}$  reaches unity (it should be pointed out that at LHC central collisions correspond to roughly three times more charged particles than those measured at RHIC). On the other side, while SPS and RHIC results show a strong centrality dependence, the  $J/\psi$   $R_{AA}$  measured at LHC shows a very mild dependence on the centrality of the collisions. It should be noted that in the ALICE results, a very low  $p_T$  cut is applied ( $p_T > 0.3$  GeV/c) in order to reject  $J/\psi$  produced via photoproduction processes (108, 109), which contribute significantly to the  $J/\psi$  yield in particular in peripheral collisions.

In the right panel of **Figure 3**, the  $R_{AA}$  evaluated at midrapidity, in the most central events, is shown as a function of the  $J/\psi$  transverse momentum. Two prominent features can be noticed in the displayed results. First, the LHC results present a clear  $p_T$  dependence. Results from different experiments show a remarkable agreement in the common  $p_T$  range, with a significant increasing suppression, when moving from the low to the high  $p_T$  region. Second, the RHIC results have a very different trend, with a  $R_{AA}$  significantly lower than

unity, but with almost no  $p_T$  dependence. The difference with respect to the LHC results is particularly striking in the low  $p_T$  region, where the LHC data show even a hint of exceeding unity.

From both the centrality and the  $p_T$  dependence, it is clear that the  $J/\psi$   $R_{AA}$  behavior strongly depends on the collision energy. The observation of strong differences between low and high energy results, in particular in central events and at low transverse momentum, suggests that different mechanisms set in when the  $\sqrt{s_{NN}}$  increases. This behavior, as it will be discussed later on, provides a strong indication of the presence not only of a suppression mechanism but also of (re)generation processes. As discussed in Section 3.2 also cold nuclear matter effects are present in AA collisions. However, as it will be addressed in Section 4, the interpretation of the results based on the interplay of suppression and (re)generation mechanisms is not altered by the presence of these cold medium effects, since their size and their centrality and  $p_T$  dependence cannot account for the observed  $J/\psi$   $R_{AA}$  behavior.

Since the distribution of charm quarks in the medium is expected to peak around  $y \simeq 0$ , reaching its maximum at low  $p_T$ , the  $J/\psi$  produced via (re)generation processes are expected to reflect such distribution, presenting a strong kinematic dependence when studied versus  $p_T$  and rapidity. Hence, the possibility of measuring charmonium down to zero transverse momentum and in two rapidity regions, a midrapidity ( $|y| < 0.9$ ) and a forward one ( $2.5 < y < 4$ ), puts the ALICE experiment (51, 110) in an ideal condition to explore the role of (re)generation in Pb–Pb collisions at LHC energies.

The  $J/\psi$   $R_{AA}$ , measured in both rapidity regions, is shown in **Figure 4** as a function of centrality ( $\langle N_{\text{part}} \rangle$ , top left), and as a function of  $p_T$  (top right). The  $J/\psi$   $R_{AA}$  shows a strong rapidity dependence, visible when studied both as a function of centrality and  $p_T$ . More in detail, the differences between the  $R_{AA}$  computed in the two rapidity regions become significant in central Pb–Pb collisions and for  $p_T < 4$  GeV/ $c$ , where the  $R_{AA}$  measured at midrapidity is close to (or even slightly exceeds) unity. Qualitatively, these observations can be interpreted as due to the (re)generation process, dominant, as previously discussed, at low  $p_T$ .

A more quantitative assessment of the role of the suppression and (re)generation mechanisms requires a comparison of the measured  $J/\psi$   $R_{AA}$  to theoretical models, as also shown in **Figure 4**. Both the SHMc (36) and the TAMU (42) calculations nicely describe the centrality dependence of the  $R_{AA}$ , while discrepancies in the high  $p_T$  range are visible, in the case of the SHMc model. As discussed in Section 2.3, the TAMU approach includes suppression and (re)generation mechanisms in a hot QGP and assumes a 20% further suppression induced by nuclear shadowing as the dominant cold nuclear matter effect. The model describes the data, with  $\sim 80\%$  of the  $J/\psi$  produced by (re)generation in central collisions at midrapidity, while this number decreases to  $\sim 50\%$  at forward rapidity. At very low  $p_T$  ( $p_T < 2$  GeV/ $c$ ) almost all the  $J/\psi$  at midrapidity are produced via (re)generation, while this fraction reduces to  $\sim 60\%$  at forward rapidity. The SHMc model nicely describes the data at low transverse momentum, while it underestimates  $R_{AA}$  at high  $p_T$ , a consequence of including only the pp-like contribution from the corona region and no  $\psi$  production in jets.

Other models (not shown in **Figure 4**) are also available and fairly describe the data (see e.g. (22, 51)). Alternative transport models, such as the one described in Ref. (54), employ slightly different implementations of the rate equation and open charm cross-section. Other approaches, such as the “comover model” (58) are based on the assumption that the modification of the charmonium yields is due to (re)generation and suppression mechanisms,

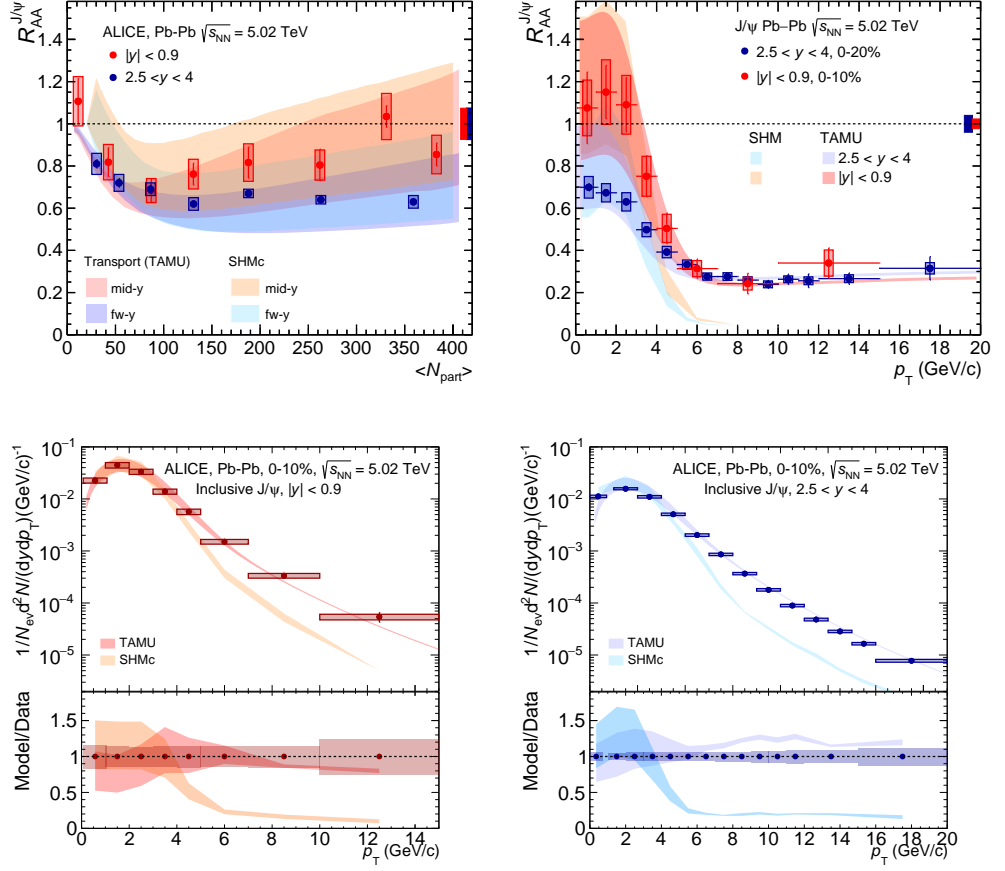


**Figure 4**

The  $J/\psi$   $R_{AA}$  measured by ALICE in  $|y| < 0.9$  and  $2.5 < y < 4$  is shown as a function of  $\langle N_{part} \rangle$  (top left) and as a function of  $p_T$ , in the most central collisions (top right). The data are compared to the SHMc (36) and TAMU (42) theory calculations. In the bottom panels, the fully corrected inclusive  $J/\psi$   $p_T$ -differential yields,  $d^2N/(dy dp_T)$  in Pb–Pb collisions are shown, at midrapidity (left) and at forward rapidity (right), in comparison to the same theory calculations. The ratio between data and models is also shown. The filled boxes around unity represent the quadratic sum of statistical and systematic uncertainties from the measurements.

with the suppression due to the interactions of the pre-resonant  $J/\psi$  state with comovers of partonic or hadronic origin, produced in the same kinematical region. In this model, the comovers density is tuned on the measured hadron yields, the dissociation cross section is tuned on low energy data, assuming no  $\sqrt{s_{NN}}$  dependence and the (re)generation effects are based on a transport equation.

The uncertainties of the models are still rather large when compared to the precision currently reached by the experimental data. This is mainly a consequence of the uncertainty on the inclusive charm cross-section for Pb–Pb collisions. The equivalent value for pp collisions, including nuclear shadowing for Pb–Pb collisions, is  $d\sigma_{cc}/dy = 0.68 \pm 0.10$  mb and  $d\sigma_{cc}/dy = 0.93 \pm 0.12$  mb for the SHMc and TAMU models, respectively.

In the bottom panels of **Figure 4**, the fully corrected inclusive  $J/\psi$   $p_T$ -differential yields,  $d^2N/(dydp_T)$  in Pb-Pb collisions are also shown, in the two rapidity ranges under study, and directly compared to the theory calculations (30, 42). The good agreement of the TAMU model and of the SHMc one, in this case in the low transverse momentum region, already observed for the  $R_{AA}$ , is confirmed in the description of the spectra. We recall that the models genuinely predict yields,  $R_{AA}$  is obtained via a normalization to the pp measurement. The SHMc calculations shown in **Figure 4** are based on a parametrized (blast wave) hydrodynamical flow (30), a calculation with a full hydrodynamical treatment of  $J/\psi$  (39) leads to a harder  $p_T$  spectrum (noticed earlier in Ref. (111)), consequently describing the data less well. It is shown in Ref. (39) that a narrower spatial distribution of (anti)charm quarks leads to a softer spectrum. A more refined treatment in hydrodynamics, including diffusion of (anti)charm quarks, is performed in Refs. (111, 112).

**3.3.2.  $J/\psi$  elliptic flow.** In parallel with the extensive studies of the  $J/\psi$   $R_{AA}$ , further insights on the behavior of charmonium in AA collisions can be inferred by measuring the  $J/\psi$  elliptic flow, evaluated through the  $v_2$  observable.

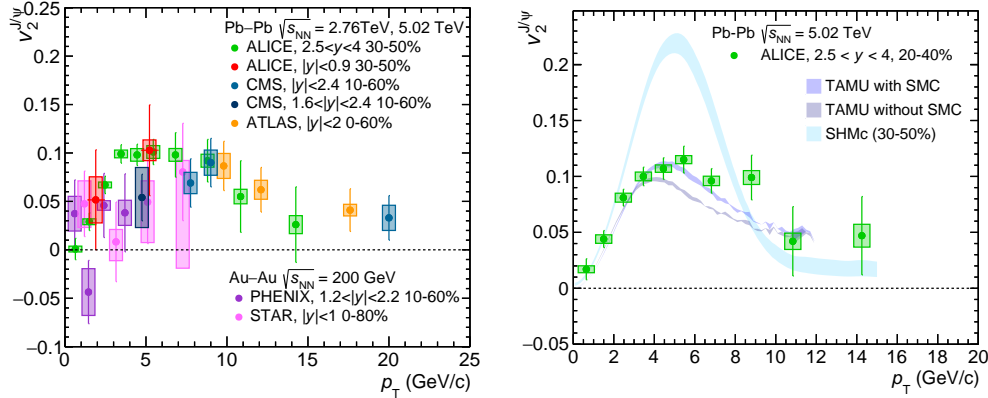


**Figure 5**

The  $p_T$ -dependence of  $J/\psi$   $v_2$  is shown, compiling results from LHC (107, 113, 114) and RHIC (115, 116) experiments (left panel). The  $p_T$ -dependence of the ALICE  $v_2$  results at forward rapidity, in the centrality interval 20-40%, is compared to theory calculations from the TAMU transport model (111) and SHMc (39) (right panel). It should be noted that the SHMc calculation is for a slightly different centrality range, i.e. 30-50%.

The compilation of all the available  $v_2$  results at RHIC at LHC energies is shown in the left panel of **Figure 5**. The study of this observable requires large luminosities and hence, as it can be seen in **Figure 5**, the level of precision is not yet optimal over the whole kinematic range and collision energies. Although the measurements included in the plot have slightly different kinematic coverage or refer to different collision energy and centrality, several features can be observed. While the elliptic flow of  $J/\psi$  was found to be compatible with zero at RHIC, with almost no  $p_T$  dependence (albeit with large uncertainties) (115, 116), the corresponding quantity measured at LHC (107, 113, 114) has a rise towards intermediate  $p_T$ , reaching a value of 0.1 in semi-central collisions and  $p_T \sim 4$  GeV/c. The behavior is explained assuming that a large fraction of the detected  $J/\psi$  originates from the (re)generation of charm quarks, which acquire their anisotropy



by taking part in the collective expansion of the system. This observation confirms once more the interpretation of the  $R_{AA}$  measurements. In the right panel of **Figure 5**, the ALICE  $v_2$  results obtained in the rapidity region  $2.5 < y < 4$ , in 20-40% centrality, are compared to the previously discussed theory models, TAMU (111) and SHMc (39). The TAMU model describes the  $v_2$  over the fully explored range, thanks to the inclusion of space-momentum correlations of the diffusing charm and anti-charm quarks in the expanding fireball. The model describes very well the data also for the high- $p_T$  region, demonstrating that (re)generation is important even at  $p_T \simeq 8 \text{ GeV}/c$ . The SHMc model predicts a rise of the  $v_2$  reaching a maximum around  $p_T \sim 5 \text{ GeV}/c$ , however, it overestimates the data significantly, underlying that the treatment in the model is currently not complete. The TAMU calculations (56) exhibit comparably large  $v_2$  values for the (re)generated  $J/\psi$ , but the inclusion of the primordial component, which dominates for  $p_T > 5 \text{ GeV}/c$ , leads to the very good description of the data. In the SHMc calculations, the large  $v_2$  values for  $p_T \simeq 8 \text{ GeV}/c$  are of purely hydrodynamic origin. For still larger  $p_T$  values  $v_2$  is likely due to path-length effects (117). The  $v_2$  measurement performed by ALICE at midrapidity (and included in the left panel of **Figure 5**) confirms the observations at forward rapidity, but the large uncertainties so far prevent further conclusions on the  $v_2$  dependence on rapidity.

**3.3.3.  $J/\psi$  polarization.** Finally, additional information on the quarkonium behavior in the QGP might be inferred by polarization measurements. First analyses from the ALICE Collaboration (118) have computed the polarization parameters in the commonly adopted helicity and Collins-Soper reference frames, in the rapidity range  $2.5 < y < 4$  in Pb-Pb collisions. The parameters  $\lambda_\theta$ ,  $\lambda_\phi$  and  $\lambda_{\theta\phi}$ , which define the degree of polarization, are found to be compatible with zero, reaching a maximum of about two standard deviations at low  $p_T$ , for both reference frames.

The degree of polarization can also be sensitive to the strong magnetic field created in the high-energy nuclear collisions, as well as to vorticity effects in the QGP. For these studies, the polarization is evaluated with respect to the event plane of the collision (119). A small transverse polarization is measured, with a significance reaching  $3.9\sigma$  at intermediate  $p_T$  ( $2 < p_T < 4 \text{ GeV}/c$ ) and intermediate centrality (30-50%). This observation is qualitatively in agreement with a similar measurement for light vector mesons (120), consistent with a possible quark polarization in the presence of a rotating fluid. However, charm quarks are produced in the early phases of the interaction when the magnetic field is stronger and hence the  $J/\psi$  polarization might be also more sensitive, compared to light quarks, to this magnetic field. A quantitative understanding of how the polarization of quarkonium is influenced and reflects the properties of the QGP medium would still require from the theory point of view, detailed calculations connecting the  $J/\psi$  production to the QGP properties and, from the experimental point of view, larger luminosities.

**3.3.4.  $\psi(2S)$  in AA collisions.** To have a complete overview of the charmonium production in heavy-ion collisions, the understanding of the role of the excited states is mandatory because, given the smaller binding energy and larger radius, they can be affected in a different way by the suppression and (re)generation mechanisms. Furthermore, since  $\sim 30\%$  of the prompt  $J/\psi$  are produced by the feed-down of the  $\psi(2S)$  and  $\chi_c$ , the understanding of their fate in the QGP allows to better interpret the fate of the directly produced  $J/\psi$ .

The measurement of the  $\chi_c$  states is rather complicated, due to the difficulties in the reconstruction of their radiative decay  $\chi_c \rightarrow J/\psi\gamma$ . First results on the  $\chi_{c1} + \chi_{c2}$  production

in pA collisions from the LHCb Collaboration have been recently released (121), but no measurement in AA are so far available.

Additionally, the  $\psi(2S)$  measurements are challenging due to its branching ratio in the dimuon channel being approximately 7.5 times lower compared to the  $J/\psi$ , as well as its production cross section in pp collisions at LHC energy being about six times smaller. Already at SPS energies, the NA50 experiment (8) had observed a stronger suppression of this resonance with respect to the  $J/\psi$ . Therefore it is important to investigate its behavior also at LHC, where competitive mechanisms such as (re)generation might be involved. While the  $\psi(2S)$  large radius and small binding energy favor its suppression with respect to the tightly bound  $J/\psi$ , the impact on the (re)generation processes on the  $\psi(2S)$  is less clear. According to the TAMU model (42), for example, the (re)generation of  $J/\psi$  and  $\psi(2S)$  is sequential, with the  $\psi(2S)$  being formed by (re)generation at lower temperatures than the  $J/\psi$ , with significant contributions not only from the QGP phase, but also from the hadronic phase. In the SHMc model both  $\psi(2S)$  and  $J/\psi$  are produced exclusively at hadronization at the QCD crossover boundary. Consequently, their relative yield is determined solely by the temperature.

Before moving to the discussion of Pb–Pb data, it should be pointed out that the  $\psi(2S)$  production shows already medium modifications in p–Pb and d–Au collisions, in particular in the backward rapidity region (92, 93, 94, 95). Initial-state cold nuclear matter effects, such as shadowing, affect in a very similar way the  $J/\psi$  and the  $\psi(2S)$ , being directly connected with the creation of the heavy-quark pair. But while the modification of the  $J/\psi$  yields can be described just with these initial-state CNM effects, in the  $\psi(2S)$  case additional final-state effects, such as interactions in a very dense medium (of hadronic or partonic origin (96, 97)) are needed to describe the data. This means that the medium created in p(d)-A collisions might already impact the yields of the loosely bound  $\psi(2S)$ .

In **Figure 6** (left panel) the relative production of  $\psi(2S)$  and  $J/\psi$  is shown as a function of  $\langle N_{\text{part}} \rangle$ . The results from the ALICE experiment (122) (in the region  $2.5 < y < 4$ ), even if limited to four centrality bins, do not show a significant centrality dependence. The NA50 (8) results at the SPS,  $\sqrt{s_{\text{NN}}} = 17.3$  GeV, on the contrary, do show a significant decrease versus centrality, being more suppressed in the most central collisions. As pointed out in Ref. (122) part of the different behavior observed in the two results could be due to the different size of the non-prompt component, almost negligible at low energy. The TAMU (123) theoretical calculation describes, within the uncertainties, the ALICE observed trend, while the SHMc (31, 36) one slightly underestimates the data in the most central collisions. We note that for the SHMc model the predictions are identical for the LHC and SPS energies, since, as already discussed, they depend on the hadronization temperature, which was observed to not change from SPS to LHC energies (31). The model describes the SPS data very well, although in this case the full screening of charmonia in QGP and exclusive generation at the hadronization may be debated. The centrality dependence of the ratio is in the SHMc determined by the superposition of the core and corona components.

When comparing results obtained at different collision energies, a common observable is the “double ratio”, i.e. the  $\psi(2S)$  to  $J/\psi$  ratio in AA, normalized to the corresponding pp one. The “double ratio” is shown in the bottom panel of **Figure 6** (left). It can be observed that the suppression of the  $\psi(2S)$  production in nucleus-nucleus collisions, with respect to the  $J/\psi$  one, is larger by roughly a factor of 2, in AA collisions compared to pp. The difference reaches a factor 5 in the most central collisions, at SPS energies.

Also the  $\psi(2S)$ , as the  $J/\psi$ , can be studied by the ALICE experiment down to zero

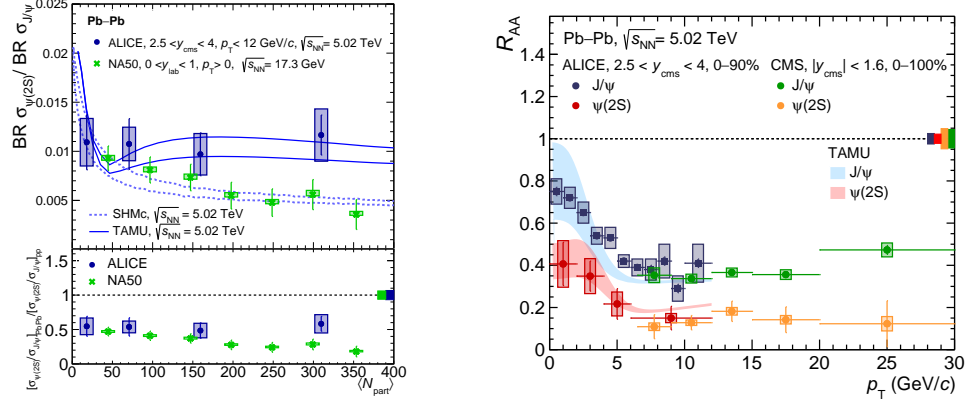


**Figure 6**

The ratio of the inclusive production cross sections of the  $\psi(2S)$  to  $J/\psi$ , not corrected for the branching ratios (B.R.) in the dimuon channels, is plotted as a function of  $\langle N_{part} \rangle$ . Results from ALICE (122) and NA50 (8), in Pb-Pb collisions are shown, together with the theoretical curves from TAMU (123) and SHMc (31, 36) at  $\sqrt{s_{NN}} = 5.02$  TeV (left panel). The  $\psi(2S)$  to  $J/\psi$  double ratio is also present in the bottom panel. A compilation of  $\psi(2S)$  and  $J/\psi$   $R_{AA}$  results is shown as a function of  $p_T$  (106, 122). The TAMU (42) theoretical calculations are also included for both resonances. It should be noted that while the ALICE results refer to inclusive charmonia, the CMS ones refer to prompt production.

transverse momentum, as visible in the right panel of **Figure 6**, where a compilation of the  $R_{AA}$  of the two mesons is shown (106, 122) as a function of  $p_T$ . The availability of results from both the ALICE and the CMS experiments allows a detailed study over an extended transverse momentum range, from zero up to 30 GeV/c. Several features are visible. First of all, the  $\psi(2S)$  and the  $J/\psi$   $R_{AA}$  follow a very similar trend, but the  $\psi(2S)$  shows a stronger suppression, by almost a factor of two, over the explored  $p_T$  range. A clear hierarchy in the  $R_{AA}$  is hence visible. Furthermore, in the low  $p_T$  region, also the  $\psi(2S)$   $R_{AA}$  has a rise towards low  $p_T$ , similar to the one observed in the  $J/\psi$ , and interpreted as due to (re)generation mechanisms. This observation hints at the conclusion that similar processes are at play also in the  $\psi(2S)$  case. Both the  $J/\psi$  and the  $\psi(2S)$   $R_{AA}$  values remain, then, almost constant up to the  $p_T$  region covered by the CMS experiment. A comparison with the predictions of the TAMU model (42) is also shown in the same plot. The model, which was already successfully describing the  $J/\psi$  nicely follows the pattern described by the  $\psi(2S)$   $R_{AA}$ , pointing out that, also in the case of this loosely bound resonance, suppression and (re)generation mechanisms are at play. According to Ref. (42), the majority of the  $\psi(2S)$  are produced by (re)generation at low  $p_T$  region, in central and semi-central collisions. The contribution of primordial  $\psi(2S)$  is relevant only for  $p_T > 5$  GeV/c, where the production by (re)generation vanishes. It should be noted that the centrality integrated results shown in the right panel of **Figure 6** exhibit a rather strong bias toward central collisions, due to the scaling with the number of collisions of the  $c\bar{c}$  pairs.

The  $\psi(2S)$  studies require large luminosities, hence other observables are still lacking precision in comparison to the  $J/\psi$  ones. For example, the  $\psi(2S)$   $v_2$  has been measured by CMS, but the result is limited to the high  $p_T$  region (114). The CMS results show a slightly

larger  $v_2$  of the  $\psi(2S)$  compared to the  $J/\psi$ , but unfortunately, the result is still limited by lack of statistics and hence not yet conclusive.

### 3.4. Bottomonium experimental results

The quarkonium study in heavy-ion collisions received a further significant boost when the first bottomonium measurements became available at the LHC.

The eagerly awaited observation, done by the CMS collaboration, of the suppression of  $\Upsilon$  mesons in Pb–Pb was a breakthrough (124). Furthermore, it was also observed that the  $\Upsilon(1S)$  suppression was significantly stronger than the one of the radially-excited states, the  $\Upsilon(2S)$  and  $\Upsilon(3S)$ , suggesting that the suppression of the three states was sequential. The first results were soon confirmed by the current more precise and differential measurements of  $R_{AA}$  for all the  $\Upsilon$  states by CMS (66, 125, 126) and ATLAS (127) at midrapidity and ALICE at forward rapidity (128).

**3.4.1.  $\Upsilon(nS)$  in AA collisions.** A compilation of the  $\Upsilon(1S)$   $R_{AA}$  results is presented in the top left panel of **Figure 7**, where all the available measurements, at several center-of-mass energies are shown as a function of the charged particle multiplicity evaluated at midrapidity. When plotted as a function of  $\langle dN/d\eta \rangle$ , contrarily to what happens in the charmonium sector, all the results follow the same trend, with the suppression magnitude and pattern similar at LHC (66, 125, 126, 127, 128) and at RHIC (129) energies. Another feature visible in the  $\Upsilon(1S)$   $R_{AA}$  pattern is a significant reduction from the peripheral to the most central events, by almost a factor 4 at LHC. It should be noted that bottomonium studies were not within reach at the SPS energies, where only a first measurement of  $\Upsilon(1S + 2S + 3S)$ , i.e. not separating the three resonances, was performed by the NA50 experiment in pA collisions (130).

The behavior of the  $\Upsilon$  states is clearly different from the charmonium one. The  $\Upsilon(1S)$  suppression not only does not show a significant energy dependence, but it also presents a similar magnitude at forward rapidity and midrapidity and a limited transverse momentum dependence, as shown in the four panels of **Figure 7**. All these features point to a limited role of the (re)generation mechanisms when b quarks are involved. The expected number of  $b\bar{b}$  pairs in central Pb–Pb collisions is about 4 in the full phase space, with about 0.6 pairs per unit of rapidity at midrapidity and a factor 2 smaller for the range  $2.5 < y < 4$ .

When comparing the  $R_{AA}$  of the three  $\Upsilon$ , the suppression is gradually stronger going from the 1S to the 2S and 3S states. This behavior can be observed both as a function of centrality (bottom panels of **Figure 7**) and as a function of the transverse momentum (top right panel). In most central collisions, the  $\Upsilon(1S)$  are suppressed by a factor  $\sim 4$ , the  $\Upsilon(2S)$  by a factor  $\sim 10$  and the  $\Upsilon(3S)$  are almost vanished. This striking pattern is denoted as “sequential suppression”. It should be noted that, since in pp collisions, up to 30–50% of the measured  $\Upsilon(1S)$  yield results from the feed-down from other states, a significant amount of  $\Upsilon(1S)$  suppression may arise from the melting of the excited states in the QGP. Together with the impact of the excited states feed-down, also cold nuclear matter effects should be taken into account when interpreting the  $\Upsilon(nS)$  modification in AA collisions. Proton-nucleus results (80, 81, 83, 132) show that effects such as shadowing, affect bottomonia, leading to a reduction of their yields. A precise measurement of the size of these effects is hence relevant to understand if even the directly produced, and strongly bound,  $\Upsilon(1S)$  melts in the QGP.

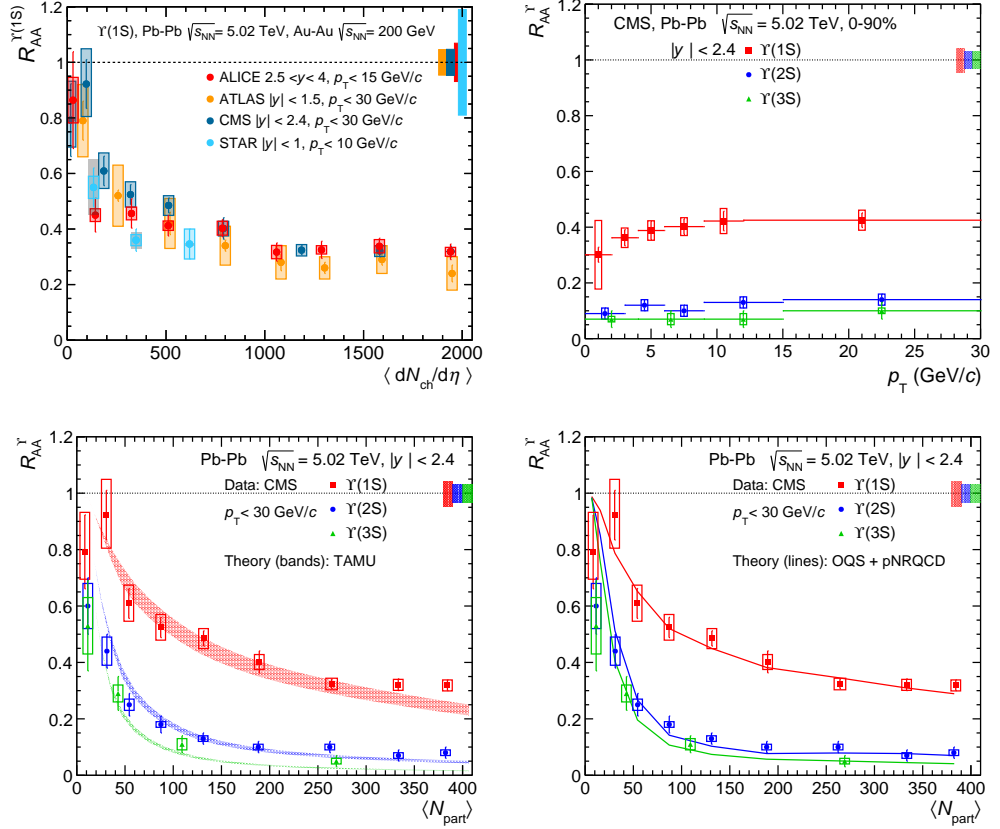


**Figure 7**

The  $\Upsilon(1S)$   $R_{AA}$  dependence on  $\langle dN_{ch}/d\eta \rangle$  for Au-Au collisions at  $\sqrt{s_{NN}} = 200$  GeV (129) and Pb-Pb at  $\sqrt{s_{NN}} = 5.02$  TeV (66, 125, 126, 127, 128) is shown (top left panel). The  $R_{AA}$  of the three  $\Upsilon(nS)$  resonances is shown as a function of  $\langle N_{part} \rangle$  and compared to theory calculations from the TAMU semiclassical transport model (131) (bottom left panel) and the OQS+pNRQCD approach of the Munich-KSU group (47) (bottom right panel). The  $p_T$  dependence of the  $R_{AA}$  of the  $\Upsilon(nS)$  states, as measured by CMS (66) is also shown (top right panel).

The comparison of bottomonium results to two theoretical models is shown in the bottom panels of **Figure 7**. It can be noticed that the models nicely describe the measurements for the whole bottomonium family. The TAMU calculations (131) include regeneration, which leads to a contribution, for instance, of about 20% for the 1S state and about 40% for the 2S state, dependent on centrality and  $p_T$ . It is worth noting that the model achieved a very good description of RHIC data at  $\sqrt{s_{NN}} = 200$  GeV, in this case with a significantly lower amount of (re)generation (131). The comparison to the OQS+pNRQCD calculations (47) is also shown. In this case as well, the inclusion of (re)generation, of a smaller amount compared to the TAMU case, improves the agreement with the data.

The data are shown as a function of  $p_T$  in **Figure 7** for midrapidity in 0-90% Pb-Pb collisions. Also in this case, the observed trend is rather different compared to the charmonium one. No prominent features were observed, except a small increase of  $R_{AA}$  vs.  $p_T$  for the  $\Upsilon(1S)$  state. The sequential suppression observed as a function of centrality

is confirmed. The theory calculations which describe the centrality dependence achieve a good description of the  $p_T$  dependence of  $R_{AA}$  (not shown here, see Ref. (66)).

**3.4.2.  $\Upsilon(1S)$  elliptic flow and polarization.** Similarly to the charmonium case, the elliptic flow of  $\Upsilon(1S)$  and  $\Upsilon(2S)$  mesons was measured at LHC energies. Even if the uncertainties are still large, the  $v_2$  turns out to be compatible with zero, both at forward rapidity (133) and at midrapidity (134). The observation of a  $v_2$  much smaller than the one measured for the  $J/\psi$  suggests a much more limited role of (re)generation in the bottomonium sector.

The ALICE Collaboration also released a first measurement of the  $\Upsilon(1S)$  polarization in Pb–Pb collisions (118). Results, integrated over rapidity and  $p_T$ , show absence of polarization, even if, also in this case, uncertainties are still rather large.

## 4. WRAP UP ON CURRENT UNDERSTANDING OF QUARKONIA IN QGP

Quarkonium is certainly one of the most prominent probes for quark-gluon plasma studies, its production being sensitive to the medium created in the collision. One of the points of strength of quarkonium is that it exists in a large variety of states, characterized by very different binding energies, from  $\sim 50$  MeV for the  $\psi(2S)$  up to  $\sim 1.1$  GeV for the  $\Upsilon(1S)$ . All these states are expected to be sensitive in a different way to the created medium, hence providing handles to understand the QGP properties. Furthermore, since quarkonium has been studied since the very beginning of the heavy ion program at SPS, many measurements are available over a broad range of collision energies, from  $\sqrt{s_{NN}} = 17$  GeV at SPS up to  $\sqrt{s_{NN}} = 5.36$  TeV at LHC and a high level of precision is now reached, in particular for the  $R_{AA}$  observable.

As discussed in the previous Sections, the main features that can be inferred from the charmonium results are the following:

- the  $J/\psi$   $R_{AA}$  shows a significant dependence on the collision energy, being more suppressed at SPS and RHIC and less suppressed at LHC energies;
- while at lower energies the  $J/\psi$  suppression is stronger in the most central collisions, at LHC energies the centrality dependence is rather mild;
- both at RHIC and LHC energies the  $J/\psi$   $R_{AA}$  shows a rapidity dependence, being more suppressed at forward rapidity than at midrapidity;
- at LHC energies, the  $J/\psi$   $p_T$  dependence is rather strong, with  $R_{AA}$  even slightly exceeding unity at low  $p_T$ , followed by a strong decrease versus high  $p_T$ ;
- at LHC, the  $J/\psi$  present also a  $v_2$  significantly different from zero, suggesting that charm quarks thermalize in the medium and take part in the collective flow;
- the loosely bound charmonium state, the  $\psi(2S)$ , shows similar features to the  $J/\psi$ , however, this resonance is more suppressed, over the whole centrality or transverse momentum range, than its ground state, by roughly a factor two.

Theory models such as the statistical hadronization or those based on transport equations provide a qualitative description of the  $R_{AA}$  and  $v_2$  results assuming an interplay of suppression and (re)generation mechanisms. At LHC energies the (re)generation process dominates for  $J/\psi$  produced at midrapidity and low transverse momentum, since this is the kinematic region where the bulk of the charm quark production is. The theoretical description of the data, with about 16  $c\bar{c}$  pairs in a QGP volume of about  $5000 \text{ fm}^3$  in central Pb–Pb collisions at midrapidity, provides a clear demonstration of deconfinement,

with charmonium production dominantly at or close to the QCD crossover boundary.

In the bottomonium sector, the main features are the following:

- the  $\Upsilon(1S)$   $R_{AA}$  shows almost no dependence on the collision energy, when results are plotted as a function of  $\langle dN_{ch}/d\eta \rangle$ ;
- at LHC energies, the  $R_{AA}$  of the three  $\Upsilon$  states shows a clear centrality dependence, being more suppressed in the most central collisions compared to the peripheral ones;
- there is a clear hierarchy in the suppression of the  $\Upsilon(nS)$  resonances, with the  $\Upsilon(1S)$   $R_{AA}$  reaching 0.4 in most central collisions, while the  $R_{AA}$  of the  $\Upsilon(2S)$  reaches 0.1 and the  $\Upsilon(3S)$  is almost vanished;
- the  $\Upsilon(1S)$   $v_2$  is almost zero, even if the measurement is still affected by large uncertainties.

Many theoretical models describe the  $\Upsilon(nS)$  measurements. They differ in the way they realize destruction and (re)generation of the  $\Upsilon$  states. Remarkable new developments include the quantum treatment of the processes, where new insights are still expected. For bottomonium, the suppression mechanism is the dominant one, even if a small amount of (re)generation might also be present. The quantitative question for the  $\Upsilon(1S)$  is if what we are observing is really the suppression of the resonance itself (whose binding energy is larger than 1 GeV), or if the decrease of the  $R_{AA}$  is the result of the suppression of the excited states having their feed-down in  $\Upsilon(1S)$ , in addition to the yield reduction induced by cold nuclear matter effects, as it will be discussed in the following.

As a final wrap-up, we can compare the  $J/\psi$  and  $\Upsilon(1S)$   $R_{AA}$  results obtained in Pb–Pb collisions at LHC, with the corresponding measurements in p–Pb. The  $R_{AA}$  as a function of the transverse momentum, as obtained by the ALICE experiment, are shown in **Figure 8**.

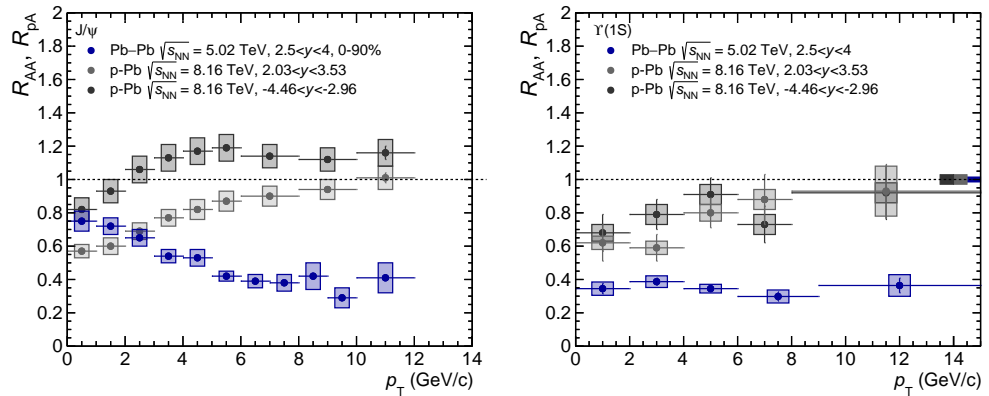


**Figure 8**

$J/\psi$  (135) and  $\Upsilon(1S)$  (128)  $R_{AA}$  as a function of  $p_T$  (left and right panels, respectively) as measured at forward rapidity ( $2.5 < y < 4$ ) in Pb–Pb collisions at  $\sqrt{s_{NN}} = 5.02$  TeV (blue symbols). The results are compared to the corresponding  $R_{pA}$  measured in pA collisions (80, 136) (gray symbols).

The pA data have been collected in two different rapidity ranges ( $2.03 < y < 3.53$  and  $-4.46 < y < -2.96$ ), corresponding to the proton or the Pb ions going towards the ALICE muon spectrometer, respectively. Despite the slightly different collision energy and kinematic range, a striking difference between the  $p_T$  dependences observed in pA and AA



data can be noticed. In particular, in the high  $p_T$  region, the pA data show a trend close to unity, suggesting a vanishing of modification effects, while Pb–Pb data present a significant reduction in the  $R_{AA}$  values. This is a clear indication that different mechanisms are at play, both for the  $J/\psi$  and for the  $\Upsilon(1S)$ .

Going one step further, a more quantitative estimate of the impact of CNM effects on the Pb–Pb data can be performed, based on the reasonable assumption that, as discussed in Ref. (80, 137, 138) and Section 3.2, cold nuclear matter effects, and in particular shadowing, are enough to describe the proton-nucleus data for quarkonium ground states. Despite the slightly different center-of-mass energy and kinematic coverage, see Ref. (137, 138), the Bjorken- $x$  ranges probed by the  $J/\psi$  production process in the two colliding Pb nuclei, assuming a  $gg \rightarrow J/\psi$  ( $2 \rightarrow 1$ ) mechanism, are only slightly shifted compared to the corresponding intervals for p–Pb and Pb–p. Hence, under the assumption that shadowing is a dominant contribution and that the CNM effects on the two colliding nuclei can be factorized, one may evaluate the shadowing contribution in Pb–Pb collisions, by computing the product  $R_{pA} \times R_{Ap}$  (137, 138). As shown in Ref. (22), the cold nuclear matter effects in Pb–Pb collisions can then be canceled out by studying the ratio  $S_{J/\psi} = R_{AA}/(R_{pA} \times R_{Ap})$ . The resulting  $S_{J/\psi}$  shows a significant  $p_T$  dependence: at high  $p_T$  a strong suppression is visible, with  $S_{J/\psi}$  values reaching  $\sim 0.3$ , while, at low  $p_T$ ,  $S_{J/\psi}$  exceeds unity.

Also in the  $\Upsilon(1S)$  case (22) the  $S_{\Upsilon(1S)}$  shows a strong  $p_T$  dependence, reaching the same level as the  $S_{J/\psi}$  at high  $p_T$ , while at low  $p_T$  it approaches unity. Again, this behavior confirms that the role of (re)generation in the bottomonium sector is less relevant, with respect to the charmonium case. However, this result does not yet confirm that the suppression observed in the  $S_{\Upsilon(1S)}$  is entirely due to the suppression of the direct  $\Upsilon(1S)$ . A precise evaluation of this suppression would require: i) a precise knowledge of the feed-down values and their transverse momentum dependence ii) the suppression values for all the excited states, i.e. the  $\Upsilon(2S)$ ,  $\Upsilon(3S)$  and all the  $\chi_b$  states. While  $R_{AA}$  results for the former  $\Upsilon$  states are available, no measurements are so far available for the  $\chi_b$ . A numerical evaluation carried on in (22) suggests that at low  $p_T$  shadowing and feed-down effects could be responsible for most of the observed  $\Upsilon(1S)$  suppression, while at high  $p_T$ , where the impact of the feed-down contribution gets larger while the CNM effects get weaker, there might be room for direct  $\Upsilon(1S)$  suppression, but uncertainties prevent strong conclusions.

In summary, from Figure 8 it can be observed that both the inclusive  $J/\psi$  and the  $\Upsilon(1S)$   $R_{AA}$  have different behavior in pA and AA collisions. Furthermore, once the CNM effects in AA, are evaluated from pA data, it is clear that cold nuclear matter effects are not enough to describe the modifications of the quarkonium yields in AA collisions. Hence the presence of hot matter effects is needed.

## 5. WHAT'S NEXT?

Almost forty years have passed since the first experiments measured quarkonium in heavy-ion collisions and, certainly, many steps forward in the understanding of its behavior have been taken. These steps have been feasible thanks to increasingly-precise sets of quarkonium data collected over a broad  $\sqrt{s_{NN}}$  range, expanding from the low SPS energies up to the top LHC ones, and to the wide kinematic region which can now be covered, combining the results from different experiments. Furthermore, while the first quarkonium measurements were limited just to the  $J/\psi$  and  $\psi(2S)$ , now also the bottomonium family is extensively studied. However, even if high-precision data are available for most of the resonances, there

are still several aspects that remain to be clarified.

At LHC energies, the charmonium P-state, the  $\chi_c$ , has not yet been studied in nucleus-nucleus collisions, given the extreme difficulty in the reconstruction of its radiative decay. The interest in the  $\chi_c$  behavior is twofold. On one side, having an intermediate binding energy between the  $J/\psi$  and the  $\psi(2S)$  it would be interesting to understand how it is affected by a deconfined medium, measuring, for example, its  $R_{AA}$  or the double ratio with respect to the ground state. On the other side, the  $\chi_c$  feed-down contribution to the  $J/\psi$  ranges between 15 and 30% (12) depending on the  $J/\psi$  transverse momentum. The measurement of the P-states should, hence, also provide additional insights on the in-medium modification of the direct  $J/\psi$ .

Similarly, a precise assessment of the bottomonium excited states and their feed-down fractions would help in understanding if the observed  $\Upsilon(1S)$  suppression is compatible with the suppression of the direct  $\Upsilon(1S)$  or if it is the result of a combination of cold nuclear matter effects and suppression of the excited bottomonium states.

Furthermore, even if not addressed in this review, in the past few years new lines of study opened up. First measurements of exotic states, such as the X(3872) have been carried on in pA (139) and AA collisions (140). The study of this state in the hot and dense matter can provide information on its still unknown nature and can shed further light on the role of (re)generation and suppression mechanisms. Current measurements are still limited by large uncertainties, preventing, for the moment, an answer, but the X(3872) studies will play a pivotal role in the physics program of the LHC experiments in the next years.

## X(3872) IN HEAVY-ION COLLISIONS

The X(3872) (also denoted  $\chi_{c1}(3872)$ ) is an exotic particle first observed by the Belle Collaboration (141). Its quantum numbers are  $J^{PC} = 1^{++}$  (142, 143), but its true nature remains unknown. Proposed hypotheses (see for example Ref. (144, 145, 146)) range from it being a charmonium state, a tetraquark state or a  $D^*(2010)^0 \bar{D}^0$  molecule.

The behavior of the X(3872) in the QGP is expected to provide insight into its internal structure. Depending on whether it is a compact object, like a tetraquark, or a loosely bound molecule, its size could vary between  $\sim 0.3$  fm and  $\sim 1.5$  fm. This distinction would result in a very different interplay between suppression and (re)generation mechanisms in the medium.

Results from the CMS experiment (140) suggest an enhancement of the X(3872)/ $\psi(2S)$  production ratio in Pb–Pb compared to pp measurement at very high  $p_T$  ( $15 < p_T < 50$  GeV/c). Similarly, albeit in a different  $p_T$  range ( $p_T > 5$  GeV/c), the LHCb Collaboration (139) has observed a smaller enhancement in pA collisions.

Both measurements clearly require larger datasets for improved precision as well as an extension towards lower transverse momentum, to increase sensitivity to mechanisms such as the (re)generation. Theoretical treatments and models are available to interpret these results and guide further investigations (147, 148).

Exciting results are expected from new experiments that will soon take data or which are proposed for the next years.

At RHIC energies, high precision data are expected from the sPHENIX experiment, the most recent among the heavy-ion experiments, which started commissioning and data taking

only in 2023. sPHENIX aims to collect high luminosity Au-Au data at top RHIC energies in 2025. These eagerly-awaited sPHENIX quarkonium measurements should allow us to improve the comparison to the results obtained at the higher LHC energies even further. In particular, the goal is to increase the precision of the bottomonium measurements, since the expected statistics should allow to separately resolve the three  $\Upsilon$  states in a kinematic range that will be comparable to the one covered at LHC.

At LHC energies, ALICE 3 (149), a new proposed experiment at CERN LHC after LS4 (LHC long shutdown 4 currently foreseen in 2034-2035), aims to improve even further the quality, so far achieved, of quarkonium results, thanks to excellent vertexing and particle identification capabilities. The plan is to perform quarkonium spectroscopy studies in heavy-ion collisions at LHC energies, studying not only the P-wave quarkonium states but also the  $\eta_c$  and  $\eta_b$  states, so far never measured.

While experiments at RHIC and LHC explore the phase diagram region at baryochemical potential ( $\mu_B$ ) close to zero, a new line of investigation will be opened by the NA60+ fixed-target experiment (150), proposed at CERN SPS. NA60+ aims to study quarkonium in the so far unexplored high- $\mu_B$  region ( $\mu_B \sim 220 - 550$  MeV).  $J/\psi$  and  $\psi(2S)$  production will be investigated in Pb-Pb collisions, via a beam energy scan, between  $6 < \sqrt{s_{NN}} < 17.3$  GeV, a region not yet covered by quarkonium studies. The large luminosity exploited by NA60+ will allow a very precise measurement of the  $J/\psi$  modification at all energies and by measuring the temperature of the system, via thermal dimuons, it will be possible to investigate the correlation between the temperature and the onset of the charmonium melting. Measurements will be performed also in pA collisions, using different A targets, simultaneously exposed to the beam. This will allow us to investigate cold nuclear matter effects in the same kinematic range and at the same energy as AA collisions.

The high- $\mu_B$  region of the QCD phase diagram will be covered also by the CBM experiment (151) at FAIR. The currently foreseen collision energies ( $\sqrt{s_{NN}} < 5$  GeV) will allow the study of sub-threshold quarkonium production in Au-Au collisions. Here, however, the theoretical concepts discussed here for the collider energies (quarkonium melting in QGP, charm-quark thermalization) will not apply for such low energies but transport model calculations are available (152).

After forty years, quarkonium studies still play a relevant role in the physics programs for the upgrades of the existing experiments or for the future ones. New very high precision results are expected to complement the plethora of measurements currently available and, together with the advances in the theory models, the points that are so far still open will be clarified.

#### SUMMARY POINTS

1. Quarkonium is a unique signature of QGP formation. The  $J/\psi$ , has been studied since the beginning of the heavy-ion program and its measurements, complemented by those of excited charmonium states and the bottomonium family, now span an extended kinematic range (from  $y = 0$  up to  $\sim 5$  and  $p_T$  from 0 up to  $\sim 50$  GeV/c) and a broad collision energy range (from  $\sqrt{s_{NN}} = 17$  GeV up to  $\sim 5$  TeV).
2. The  $J/\psi$  production in Pb-Pb collisions exhibits modifications relative to that in pp collisions, scaled by the number of binary nucleon-nucleon collisions ( $R_{AA}$ ). These modifications strongly depend on the kinematic range ( $y$  and  $p_T$ ) as well as on the collision energy:

- at SPS and RHIC energies, the  $R_{AA}$  shows a significant dependence on centrality, in contrast, at LHC, the values are larger and exhibit a milder centrality dependence;
  - the  $R_{AA}$  has a clear rapidity dependence, with stronger suppression at forward rapidity compared to midrapidity;
  - at LHC energies, the  $R_{AA}$  varies significantly with  $p_T$ , being strongly suppressed at high  $p_T$  but rising at low  $p_T$ , even exceeding unity at midrapidity
3. The loosely bound  $\psi(2S)$  exhibits similar features to the  $J/\psi$ , but with an  $R_{AA}$  reduction approximately twice as strong, indicating a hierarchy in nuclear modifications.
  4. In the bottomonium sector, a clear sequential suppression is observed, with the suppression becoming progressively stronger from the  $\Upsilon(1S)$  to the  $\Upsilon(3S)$ . Unlike the charmonium case, at LHC energies, the  $R_{AA}$  exhibits a pronounced centrality dependence and a rather flat trend as a function of  $p_T$ . These features point to a dominant role for suppression mechanisms, with a more limited contribution from (re)generation processes.
  5. At the LHC, a significant  $v_2$  is observed for the  $J/\psi$ , attributed to the collective flow inherited from thermalized charm quarks. In contrast, for the  $\Upsilon(1S)$ , the  $v_2$  is consistent with zero, although the uncertainties are large.
  6. Theoretical models, such as the statistical hadronization model and those based on transport equations, either semiclassical or in the open-quantum systems approach, successfully describe many aspects of quarkonium behavior. In these models, the  $R_{AA}$  reflects the interplay between suppression mechanisms in the hot and dense deconfined medium and (re)generation processes. (Re)generation predominantly drives  $J/\psi$  production at low  $p_T$  and midrapidity, where the majority of charm quarks are produced. Genuine quantum effects, in particular for bottomonium production, have been already explored and will continue to bring theoretical insight.
  7. Quarkonium production in QGP is deeply related to the total abundances of heavy quarks; the heavy-quark diffusion process plays a crucial role in the theoretical modeling of quarkonium production in the strongly-coupled deconfined medium.
  8. The precision achieved in most of the quarkonium measurements is already very good. However, several open questions remain. Addressing these questions will require future data-taking at existing experiments, some of which will undergo significant upgrades soon, and measurements at the next generation of experiments such as ALICE 3 and NA60+, which will cover the region in the QCD phase diagram from low to high  $\mu_B$ .

## DISCLOSURE STATEMENT

The authors are not aware of any affiliations, memberships, funding, or financial holdings that might be perceived as affecting the objectivity of this review.

## ACKNOWLEDGMENTS

We acknowledge discussions with N. Brambilla, P.-B. Gossiaux, P. Petreczky, R. Rapp.

## LITERATURE CITED

1. Matsui T, Satz H. *Phys. Lett. B* 178:416–422 (1986)
2. Busza W, Rajagopal K, van der Schee W. *Ann. Rev. Nucl. Part. Sci.* 68:339–376 (2018)
3. Harris JW, Müller B. *Eur. Phys. J. C* 84(3):247 (2024)
4. Digal S, Petreczky P, Satz H. *Phys. Rev. D* 64:094015 (2001)
5. Karsch F, Kharzeev D, Satz H. *Phys. Lett. B* 637:75–80 (2006)
6. Alessandro B, et al. *Eur. Phys. J. C* 39:335–345 (2005)
7. CERN News. New state of matter created at cern, <https://home.cern/news/press-release/cern/new-state-matter-created-cern> (2000)
8. Alessandro B, et al. *Eur. Phys. J. C* 49:559–567 (2007)
9. Braun-Munzinger P, Stachel J. *Phys. Lett. B* 490:196–202 (2000)
10. Thews RL, Schroedter M, Rafelski J. *Phys. Rev. C* 63:054905 (2001)
11. Andronic A, Braun-Munzinger P, Redlich K, Stachel J. *Nucl. Phys. A* 789:334–356 (2007)
12. Lansberg JP. *Phys. Rept.* 889:1–106 (2020)
13. Boyd J, Thapa S, Strickland M. *Phys. Rev. D* 108(9):094024 (2023)
14. Acharya S, et al. *JHEP* 03:190 (2022)
15. Aaij R, et al. *JHEP* 11:181 (2021)
16. Mocsy A, Petreczky P, Strickland M. *Int. J. Mod. Phys. A* 28:1340012 (2013)
17. He M, van Hees H, Rapp R. *Prog. Part. Nucl. Phys.* 130:104020 (2023)
18. Bazavov A, Hoyer D, Larsen RN, Mukherjee S, Petreczky P, et al. *Phys. Rev. D* 109(7):074504 (2024)
19. Kluberg L, Satz H. *Landolt-Börnstein I* 23 (2010)
20. Rothkopf A. *Phys. Rept.* 858:1–117 (2020)
21. Du X, Liu SYF, Rapp R. *Phys. Lett. B* 796:20–25 (2019)
22. Acharya S, et al. *Eur. Phys. J. C* 84(8):813 (2024)
23. Dong X, Lee YJ, Rapp R. *Ann. Rev. Nucl. Part. Sci.* 69:417–445 (2019)
24. Apolinário L, Lee YJ, Winn M. *Prog. Part. Nucl. Phys.* 127:103990 (2022)
25. Das SK, Torres-Rincon JM, Rapp R. *arXiv:2406.13286* (2024)
26. Zhao J, Zhou K, Chen S, Zhuang P. *Prog. Part. Nucl. Phys.* 114:103801 (2020)
27. Rapp R, Blaschke D, Crochet P. *Prog. Part. Nucl. Phys.* 65:209–266 (2010)
28. Andronic A, et al. *Eur. Phys. J. A* 60(4):88 (2024)
29. Braun-Munzinger P, Stachel J. *Landolt-Börnstein I* 23:424 (2010)
30. Andronic A, Braun-Munzinger P, Köhler MK, Mazeliauskas A, Redlich K, et al. *JHEP* 07:035 (2021)
31. Andronic A, Braun-Munzinger P, Redlich K, Stachel J. *Nature* 561(7723):321–330 (2018)
32. Bazavov A, et al. *Phys. Lett. B* 795:15–21 (2019)
33. Borsanyi S, Fodor Z, Guenther JN, Kara R, Katz SD, et al. *Phys. Rev. Lett.* 125(5):052001 (2020)
34. Cleymans J, Redlich K, Suhonen E. *Z. Phys. C* 51:137–141 (1991)
35. Gorenstein MI, Kostyuk A, Stoecker H, Greiner W. *Phys. Lett. B* 509:277–282 (2001)
36. Andronic A, Braun-Munzinger P, Köhler MK, Redlich K, Stachel J. *Phys. Lett. B* 797:134836 (2019)
37. Braun-Munzinger P, Redlich K. *Eur. Phys. J. C* 16:519–525 (2000)
38. d’Enterria D, Loizides C. *Ann. Rev. Nucl. Part. Sci.* 71:315–344 (2021)
39. Andronic A, Braun-Munzinger P, Brunßen H, Crkovská J, Stachel J, et al. *JHEP* 10:229 (2024)

40. Andronic A, Braun-Munzinger P, Redlich K, Stachel J. *Acta Phys. Polon. Supp.* 16(1):1–A107 (2023)
41. Grandchamp L, Rapp R. *Phys. Lett. B* 523:60–66 (2001)
42. Wu B, Rapp R. *Universe* 10(6):244 (2024)
43. Tang Z, Mukherjee S, Petreczky P, Rapp R. arXiv:2411.09132 (2024)
44. Larsen R, Meinel S, Mukherjee S, Petreczky P. *Phys. Lett. B* 800:135119 (2020)
45. Brambilla N, Magorsch T, Strickland M, Vairo A, Vander Griend P. *Phys. Rev. D* 109(11):114016 (2024)
46. Delorme S, Katz R, Gousset T, Gossiaux PB, Blaizot JP. *JHEP* 06:060 (2024)
47. Brambilla N, Escobedo MA, Islam A, Strickland M, Tiwari A, et al. *Phys. Rev. D* 108(1):L011502 (2023)
48. Rapp R, Du X. *Nucl. Phys. A* 967:216–224 (2017)
49. Akamatsu Y. *Prog. Part. Nucl. Phys.* 123:103932 (2022)
50. Brambilla N, Pineda A, Soto J, Vairo A. *Nucl. Phys. B* 566:275 (2000)
51. Acharya S, et al. *Phys. Lett. B* 849:138451 (2024)
52. Klasen M, Paukkunen H. *Annual Review of Nuclear and Particle Science* 74(Volume 74, 2024):49–87 (2024)
53. Zhao X, Rapp R. *Nucl. Phys. A* 859:114–125 (2011)
54. Zhou K, Xu N, Xu Z, Zhuang P. *Phys. Rev. C* 89(5):054911 (2014)
55. Acharya S, et al. *JHEP* 01:174 (2022)
56. He M, Rapp R. *Phys. Lett. B* 795:117–121 (2019)
57. Acharya S, et al. *JHEP* 12:086 (2023)
58. Ferreiro EG. *Phys. Lett. B* 731:57–63 (2014)
59. Ferreiro EG, Lansberg JP. *JHEP* 10:094 (2018), [Erratum: *JHEP* 03, 063 (2019)]
60. Song T, Aichelin J, Zhao J, Gossiaux PB, Bratkovskaya E. *Phys. Rev. C* 108(5):054908 (2023)
61. Wolschin G. *Int. J. Mod. Phys. A* 35(29):2030016 (2020)
62. Blaizot JP, Escobedo MA. *Phys. Rev. D* 104(5):054034 (2021)
63. Yao X, Ke W, Xu Y, Bass SA, Müller B. *JHEP* 01:046 (2021)
64. Villar DYA, Zhao J, Aichelin J, Gossiaux PB. *Phys. Rev. C* 107(5):054913 (2023)
65. Chen G, Chen B, Zhao J. *Eur. Phys. J. C* 84(8):869 (2024)
66. Tumasyan A, et al. *Phys. Rev. Lett.* 133(2):022302 (2024)
67. Faccioli P, Lourenco C, Seixas J, Wohri HK. *Eur. Phys. J. C* 69:657–673 (2010)
68. Andronic A, et al. *Eur. Phys. J. C* 76(3):107 (2016)
69. Alessandro B, et al. *Eur. Phys. J. C* 48:329 (2006)
70. Alessandro B, et al. *Eur. Phys. J. C* 33:31–40 (2004)
71. Arnaldi R, et al. *Phys. Lett. B* 706:263–267 (2012)
72. Eskola KJ, Paakkinen P, Paukkunen H, Salgado CA. *Eur. Phys. J. C* 77(3):163 (2017)
73. Kovarik K, et al. *Phys. Rev. D* 93(8):085037 (2016)
74. Iancu E, Venugopalan R. hep-ph/0303204 (2003)
75. Arleo F, Peigne S. *JHEP* 03:122 (2013)
76. Alessandro B, et al. *Phys. Lett. B* 553:167–178 (2003)
77. Adare A, et al. *Phys. Rev. C* 87(3):034904 (2013)
78. Hufner J, Ivanov YP, Kopeliovich BZ, Tarasov AV. *Phys. Rev. D* 62:094022 (2000)
79. Kharzeev D, Thews RL. *Phys. Rev. C* 60:041901 (1999)
80. Acharya S, et al. *Phys. Lett. B* 806:135486 (2020)
81. Aaboud M, et al. *Eur. Phys. J. C* 78(3):171 (2018)
82. Tumasyan A, et al. *Phys. Lett. B* 835:137397 (2022)
83. Aaij R, et al. *JHEP* 11:194 (2018), [Erratum: *JHEP* 02, 093 (2020)]
84. Acharya UA, et al. *Phys. Rev. C* 105(6):064912 (2022)
85. Acharya U, et al. *Phys. Rev. C* 102(1):014902 (2020)
86. Abdallah M, et al. *Phys. Lett. B* 825:136865 (2022)

87. Albacete JL, et al. *Nucl. Phys. A* 972:18–85 (2018)
88. Vogt R. 2019. In *18th Conference on Elastic and Diffractive Scattering*
89. Strickland M, Thapa S, Vogt R. *Phys. Rev. D* 109(9):096016 (2024)
90. Du X, Rapp R. *JHEP* 03:015 (2019)
91. Adam J, et al. *JHEP* 06:050 (2016)
92. Abelev BB, et al. *JHEP* 12:073 (2014)
93. Acharya S, et al. *JHEP* 07:237 (2020)
94. Aaij R, et al. *JHEP* 03:133 (2016)
95. Adare A, et al. *Phys. Rev. C* 95(3):034904 (2017)
96. Ma YQ, Venugopalan R, Watanabe K, Zhang HF. *Phys. Rev. C* 97(1):014909 (2018)
97. Ferreiro EG. *Phys. Lett. B* 749:98–103 (2015)
98. Araldi R. *J. Phys. G* 35:104133 (2008)
99. Kharzeev D, Lourenco C, Nardi M, Satz H. *Z. Phys. C* 74:307–318 (1997)
100. Capella A, Ferreiro EG, Kaidalov AB. *Phys. Rev. Lett.* 85:2080–2083 (2000)
101. Blaizot JP, Ollitrault JY. *Phys. Rev. Lett.* 77:1703–1706 (1996)
102. Adare A, et al. *Phys. Rev. Lett.* 98:232301 (2007)
103. Adare A, et al. *Phys. Rev. C* 84:054912 (2011)
104. Adamczyk L, et al. *Phys. Rev. C* 90(2):024906 (2014)
105. Adam J, et al. *Phys. Lett. B* 797:134917 (2019)
106. Sirunyan AM, et al. *Eur. Phys. J. C* 78(6):509 (2018), [Erratum: *Eur.Phys.J.C* 83, 145 (2023)]
107. Aaboud M, et al. *Eur. Phys. J. C* 78(9):784 (2018)
108. Abelev B, et al. *Phys. Lett. B* 718:1273–1283 (2013)
109. Acharya S, et al. *Eur. Phys. J. C* 81(8):712 (2021)
110. Adam J, et al. *Phys. Lett. B* 766:212–224 (2017)
111. He M, Wu B, Rapp R. *Phys. Rev. Lett.* 128(16):162301 (2022)
112. Capellino F, Dubla A, Floerchinger S, Grossi E, Kirchner A, Masciocchi S. *Phys. Rev. D* 108(11):116011 (2023)
113. Acharya S, et al. *Phys. Rev. Lett.* 119(24):242301 (2017)
114. Tumasyan A, et al. *JHEP* 10:115 (2023)
115. Abdulameer NJ, et al. arXiv:2409.12756 (2024)
116. Adamczyk L, et al. *Phys. Rev. Lett.* 111(5):052301 (2013)
117. Noronha-Hostler J, Betz B, Noronha J, Gyulassy M. *Phys. Rev. Lett.* 116(25):252301 (2016)
118. Acharya S, et al. *Phys. Lett. B* 815:136146 (2021)
119. Acharya S, et al. *Phys. Rev. Lett.* 131(4):042303 (2023)
120. Acharya S, et al. *Phys. Rev. Lett.* 125(1):012301 (2020)
121. Aaij R, et al. *Phys. Rev. Lett.* 132(10):102302 (2024)
122. Acharya S, et al. *Phys. Rev. Lett.* 132(4):042301 (2024)
123. Du X, Rapp R. *Nucl. Phys. A* 943:147–158 (2015)
124. Chatrchyan S, et al. *Phys. Rev. Lett.* 109:222301 (2012), [Erratum: *Phys.Rev.Lett.* 120, 199903 (2018)]
125. Sirunyan AM, et al. *Phys. Rev. Lett.* 120(14):142301 (2018)
126. Sirunyan AM, et al. *Phys. Lett. B* 790:270–293 (2019)
127. Aad G, et al. *Phys. Rev. C* 107(5):054912 (2023)
128. Acharya S, et al. *Phys. Lett. B* 822:136579 (2021)
129. Aboona B, et al. *Phys. Rev. Lett.* 130(11):112301 (2023)
130. Alessandro B, et al. *Phys. Lett. B* 635:260–269 (2006)
131. Du X, He M, Rapp R. *Phys. Rev. C* 96(5):054901 (2017)
132. Chatrchyan S, et al. *JHEP* 04:103 (2014)
133. Acharya S, et al. *Phys. Rev. Lett.* 123(19):192301 (2019)
134. Sirunyan AM, et al. *Phys. Lett. B* 819:136385 (2021)
135. Acharya S, et al. *JHEP* 02:041 (2020)



136. Acharya S, et al. *JHEP* 07:160 (2018)
137. Abelev BB, et al. *JHEP* 02:073 (2014)
138. Adam J, et al. *JHEP* 06:055 (2015)
139. Aaij R, et al. *Phys. Rev. Lett.* 132(24):242301 (2024)
140. Sirunyan AM, et al. *Phys. Rev. Lett.* 128(3):032001 (2022)
141. Choi SK, et al. *Phys. Rev. Lett.* 91:262001 (2003)
142. Abulencia A, et al. *Phys. Rev. Lett.* 98:132002 (2007)
143. Aaij R, et al. *Phys. Rev. Lett.* 110:222001 (2013)
144. Tornqvist NA. *Phys. Lett. B* 590:209–215 (2004)
145. Maiani L, Piccinini F, Polosa AD, Riquer V. *Phys. Rev. D* 71:014028 (2005)
146. Hanhart C, Kalashnikova YS, Nefediev AV. *Eur. Phys. J. A* 47:101–110 (2011)
147. Wu B, Du X, Sibila M, Rapp R. *Eur. Phys. J. A* 57(4):122 (2021), [Erratum: *Eur.Phys.J.A* 57, 314 (2021)]
148. Armesto N, Ferreiro EG, Escobedo MA, López-Pardo V. *Phys. Lett. B* 854:138760 (2024)
149. ALICE. Collaboration, Letter of intent for ALICE 3: A next-generation heavy-ion experiment at the LHC, arXiv:2211.02491, CERN-LHCC-2022-009, LHCC-I-038 (2022)
150. Ahdida C, et al. Letter of Intent: the NA60+ experiment, arXiv:2212.14452, CERN-SPSC-2022-036 / SPSC-I-259 (2022)
151. Ablyazimov T, et al. *Eur. Phys. J. A* 53(3):60 (2017)
152. Cassing W, Bratkovskaya EL, Sibirtsev A. *Nucl. Phys. A* 691:753–778 (2001)